

ENERGY STABLE AND STRUCTURE-PRESERVING SCHEMES FOR THE STOCHASTIC GALERKIN SHALLOW WATER EQUATIONS

DIHAN DAI, YEKATERINA EPSHTEYN AND AKIL NARAYAN

ABSTRACT. The shallow water flow model is widely used to describe water flows in rivers, lakes, and coastal areas. Accounting for uncertainty in the corresponding transport-dominated nonlinear PDE models presents theoretical and numerical challenges that motivate the central advances of this paper. Starting with a spatially one-dimensional hyperbolicity-preserving, positivity-preserving stochastic Galerkin formulation of the parametric/uncertain shallow water equations, we derive an entropy-entropy flux pair for the system. We exploit this entropy-entropy flux pair to construct structure-preserving second-order energy conservative, and first- and second-order energy stable finite volume schemes for the stochastic Galerkin shallow water system. The performance of the methods is illustrated on several numerical experiments.

Keywords: stochastic Galerkin method, finite volume method, structure-preserving discretization, shallow water equations, hyperbolic systems of conservation law and balance laws.

AMS subject classifications: 35L65, 35Q35, 35R60, 65M60, 65M70, 65M08

1. INTRODUCTION

The one-dimensional Saint-Venant system of shallow water equations (SWE) is a popular model of water flows where vertical length scales are much smaller than horizontal ones [1]. This system in conservative form is given by,

$$(1.1) \quad U_t + F(U)_x = S(U), \quad U = (h, q)^\top \in \mathbb{R}^2,$$

where $U = U(x, t)$ is the vector of conservative variables; $h(x, t)$ is the water height (a mass-like variable) and $q(x, t)$ is the water discharge (a momentum-like variable). The flux F and source term S are given by,

$$(1.2) \quad F(U) = \begin{pmatrix} q \\ \frac{(q)^2}{h} + \frac{gh^2}{2} \end{pmatrix}, \quad S(U) = \begin{pmatrix} 0 \\ -ghB' \end{pmatrix}.$$

where $B(x)$ is the (assumed known) bottom topography function and $g > 0$ is the gravitational constant. The system (1.1) is supplemented with initial and boundary data that we omit for the time being.

The one-dimensional SWE model (1.1) is hyperbolic system of partial differential equations (PDE) if $h > 0$, and hence with the non-zero source S , then (1.1) is a nonlinear hyperbolic balance law. Because of this, it inherits the standard challenges in developing numerical methods for such models: solutions generically develop discontinuities in finite time even with smooth initial data, non-uniqueness of weak solutions should be rectified by an implicit or explicit numerical imposition of entropy conditions, and implicit time-integration solvers are challenging to implement due to the nonlinearity [8, 21, 22]. In addition to all this, the SWE has challenges that are somewhat specific to its particular form: positivity of the water height h should be maintained, and numerical schemes should accurately capture near-equilibrium dynamics, which is typically achieved by imposing the *well-balanced* property [3], i.e., that the PDE equilibrium states are exactly captured at the discrete level.

A more nebulous and hence more frustrating challenge is that of *uncertainty* in the model. For example, one may have incomplete, partial information about the initial data or the bottom topography function B . In such cases, one frequently models this data as a random variable or process, and hence the solution U to (1.1) is random. We consider the somewhat more simple situation when the input uncertainty is encoded with a finite-dimensional random variable, in which case (1.1) becomes a parametric model (with the input random variables serving as the parameters). Even with this simplification, the parametric or stochastic nature of the solution exacerbates many of the previously described numerical challenges. A particularly successful approach for handling such problems that we will employ is the polynomial Chaos (PC) method, wherein U is approximated as a polynomial function of the input parameters [34, 25, 26].

The class of *non-intrusive* PC strategies construct the polynomial by collecting an ensemble of solutions to (1.1) at a collection of fixed values of the parameters. This approach is attractive since it can exploit existing and trusted legacy solvers for (1.1), for which there are several effective choices [35, 24, 36, 32, 33, 19, 31, 29, 23, 4, 20, 30, 12, 18]. However, this approach suffers from the disadvantage that making concrete statements about the quality or properties of the resulting polynomial approximation can be challenging. For example, one cannot guarantee that entropy conditions are satisfied if the polynomial approximation is evaluated away from the parameter ensemble used to construct the approximation.

This paper is concerned with an alternative *intrusive* approach, the stochastic Galerkin (SG) method for PC approximation, which addresses the parametric dependence in a Galerkin fashion, e.g., by enforcing that certain probabilistic moments of (1.1) vanish. This approach has the potential to provide pathways to mathematical rigor of numerical methods through weak enforcement of the parametric dependence. SG methods transform a parametric model (1.1) into a new non-parametric model of larger system size. Since the new SG formulation is non-parametric, one can apply typical deterministic numerical methods for systems of PDEs to solve the SG problem. Such approaches have shown particular success for modeling parametric dependence in elliptic problems; see, e.g., [7]. However, the notable drawback of SG methods when applied to (nonlinear) hyperbolic PDEs is that the new non-parametric SG system need not be a hyperbolic PDE itself, which changes the essential character of the SG system relative to the original system. Recent work has developed an SG formulation for the SWE in conservative form that involves a special SG treatment for the nonlinear, non-polynomial terms [9]. Such an approach can be used to develop a well-balanced, hyperbolicity-preserving, and positivity-preserving finite volume method to solve the SG SWE system. This approach has also been extended to two-dimensional SWE systems [10].

1.1. Contributions of this article. We make the following contributions that build on [9]:

- We derive an entropy-entropy flux pair for the spatially one-dimensional hyperbolicity-preserving, positivity-preserving SG SWE system derived in [9], see theorem 3.1. Entropy-entropy flux pairs are the theoretical starting point for proposing entropy admissibility criteria to resolve non-uniqueness of weak solutions.
- Using the entropy-entropy flux pair, we devise second-order energy conservative, and first- and second-order energy stable finite volume schemes for the SG SWE, all of which are also well-balanced. See theorems 4.1 to 4.3, with the procedure in algorithm 1. The designed energy conservative and energy stable schemes are the stochastic extensions of the schemes developed in [15, 16].
- We provide numerical experiments that explore the simulation capabilities of the new schemes. To the best of our knowledge, these are the first schemes for any SG SWE system that boast energy stability, the well-balanced property, while also being positivity- and hyperbolicity-preserving.

An outline of this paper is as follows: Section 2 introduces our notation, along with background on PC methods and the SG SWE system from [9]. Section 3 provides our entropy-entropy pair construction for the SG SWE system. Section 4 provides the statement of the energy conservative and energy stable schemes that we develop, along with proofs of their theoretical properties, as well as their algorithmic details. Section 5 compiles numerical examples that demonstrate the performance

of our scheme. Section 6 gives brief summary of the main results and some future research directions. We summarize our notation in this article in table 1.

K	number of terms in PCE expansion,
$\widehat{U} = (\widehat{h}^\top, \widehat{q}^\top)^\top \in \mathbb{R}^K \times \mathbb{R}^K$	PCE state vector and its components for 1D SG SWE,
$U = (\mathbf{h}^\top, \mathbf{q}^\top)^\top \in \mathbb{R}^K \times \mathbb{R}^K$	quantities related to cell averages/reconstructed values, etc. of the PCE state vector and its components for 1D SG SWE,
(E, H)	entropy pair for 1D SG SWE,
\widehat{u}	PCE vector for velocity,
\mathbf{u}	quantity related to cell averages/reconstructed values, etc. of the PCE vector for velocity,
\widehat{V}, \mathbf{V}	the PCE vector for the entropic variable and quantities related to cell averages/reconstructed values, etc. of the entropic variable,
$\mathcal{P}(\cdot)$	the operator that maps a PCE vector to a PCE triple-product matrix.
$\overline{\mathbf{h}}_{i+\frac{1}{2}}$	arithmetic average of \mathbf{h}_i and \mathbf{h}_{i+1} . Similar notation is applied to other bold letters, e.g. $\overline{U}_{i+\frac{1}{2}}$.
$\llbracket \mathbf{h} \rrbracket_{i+\frac{1}{2}}$	first-order jump defined via cell averages,
$\langle\langle \mathbf{h} \rangle\rangle_{i+\frac{1}{2}}$	(notationally) second-order jump defined via reconstructed values.
\widehat{F}	flux,
\mathcal{F}	numerical flux,
Q^{EC}, Q^{ES1}, Q^{ES2}	energy-conservative flux, 1st-order energy-stable flux, and 2nd-order energy stable flux, respectively,
w^\pm, \widetilde{w}^\pm	scaled variables,

TABLE 1. Notation and terminology used throughout this article.

2. PRELIMINARIES

2.1. Notation. We use $\|\cdot\|$ to denote the standard Euclidean (ℓ^2) norm operating on vectors. If $f : \mathbb{R}^m \rightarrow \mathbb{R}^n$ for $m, n \in \mathbb{N}$, then we write $f(x)$ for $x = (x_1, \dots, x_m)$, and $f(x) = (f_1, \dots, f_n)$. We use the following notation for the gradient:

$$f_x := \frac{\partial f}{\partial x} = \begin{pmatrix} \frac{\partial f_1}{\partial x_1} & \frac{\partial f_1}{\partial x_2} & \dots & \frac{\partial f_1}{\partial x_m} \\ \frac{\partial f_2}{\partial x_1} & \frac{\partial f_2}{\partial x_2} & \dots & \frac{\partial f_2}{\partial x_m} \\ \vdots & \vdots & \ddots & \vdots \\ \frac{\partial f_n}{\partial x_1} & \frac{\partial f_n}{\partial x_2} & \dots & \frac{\partial f_n}{\partial x_m} \end{pmatrix} \in \mathbb{R}^{n \times m}.$$

When $n = 1$ (i.e., f is scalar-valued) then $\frac{\partial^2 f}{\partial x^2}$ is the $n \times n$ Hessian of f . If \mathbf{A} is a square matrix, then we write $\mathbf{A} > 0$ and $\mathbf{A} \geq 0$ when \mathbf{A} is positive definite and positive semi-definite, respectively.

In work on the SWE system (1.1) it is common to introduce the water velocity (equilibrium) variable

$$(2.1) \quad u := \frac{q}{h},$$

and we also make use of this variable in what follows.

2.2. Polynomial Chaos Expansion. In this section, we briefly review the results and notation for polynomial chaos expansion. More comprehensive results can be found in [11, 34, 26], etc.

Let $\xi \in \mathbb{R}^d$ be a random variable associated with Lebesgue density function ρ . Define the function space

$$L_\rho^2(\mathbb{R}^d) := \left\{ f : \mathbb{R}^d \rightarrow \mathbb{R} \mid \left(\int_{\mathbb{R}^d} f^2(s) \rho(s) ds \right)^{\frac{1}{2}} < +\infty \right\}.$$

Assuming finite polynomial moments of all orders for ρ , there exists an orthonormal basis $\{\phi_k\}_{k=1}^\infty$ of L_ρ^2 , i.e.,

$$(2.2) \quad \langle \phi_k, \phi_\ell \rangle_\rho := \int_{\mathbb{R}^d} \phi_k(s) \phi_\ell(s) \rho(s) ds = \delta_{k,\ell}, \quad \phi_1(\xi) \equiv 1,$$

for all $k, \ell \in \mathbb{N}$, where $\delta_{k,\ell}$ is the Kronecker delta. PCE seeks a representation of a random field $z(\cdot, \cdot, \xi) \in L^2_\rho$ in terms of a series of orthonormal polynomials for ξ ,

$$(2.3) \quad z(x, t, \xi) \stackrel{L^2_\rho}{=} \sum_{k=1}^{\infty} \widehat{z}_k(x, t) \phi_k(\xi),$$

where x, t are the deterministic spatial and temporal variables, and $\widehat{z}_k(x, t)$ are deterministic Fourier-like coefficients. The equation (2.3) holds true for all $z(x, t; \cdot) \in L^2_\rho$ under mild conditions [13]. In practice, a finite truncation of (2.3) is usually considered. Let P be a K -dimensional polynomial subspace of L^2_ρ ,

$$(2.4) \quad P = \text{span} \{ \phi_k, \quad k = 1, \dots, K \},$$

i.e., we let ϕ_k be an orthonormal basis for P . We make the common assumption that $1 \in P$, and for convenience we assume that,

$$\phi_1(\xi) \equiv 1.$$

A popular choice for P is the total degree space, but several other options are possible.

The K -term PCE *approximation* of a random field z onto P is defined by the projection of (2.3) onto P :

$$(2.5) \quad \Pi_P[z](x, t, \xi) := \sum_{k=1}^K \widehat{z}_k(x, t) \phi_k(\xi).$$

Using the orthogonality of the basis function, the statistics of $\Pi_P[z]$ can be expressed in terms of the expansion coefficients. For example, the mean and the variance of $\Pi_P[z]$ are given by:

$$(2.6) \quad \mathbb{E}[\Pi_P[z](x, t, \xi)] = \widehat{z}_1(x, t), \quad \text{Var}[\Pi_P[z](x, t, \xi)] = \sum_{k=2}^K \widehat{z}_k^2(x, t).$$

Let $\widehat{z} = (\widehat{z}_1, \dots, \widehat{z}_K) \in \mathbb{R}^K$ be the vector of the expansion coefficients in (2.6). Define the linear operator $\mathcal{P} : \mathbb{R}^K \rightarrow \mathbb{R}^{K \times K}$ as

$$(2.7) \quad \mathcal{P}(\widehat{z}) := \sum_{k=1}^K \widehat{z}_k \mathcal{M}_k, \quad \mathcal{M}_k \in \mathbb{R}^{K \times K}, \quad (\mathcal{M}_k)_{\ell, m} = \langle \phi_k, \phi_\ell \phi_m \rangle_\rho.$$

Fixing $\widehat{z} \in \mathbb{R}^K$, then $\mathcal{P}(\widehat{z})$ is the (symmetric) quadratic form matrix representation of the bilinear operator $(\widehat{a}, \widehat{b}) \mapsto \langle a_P z_P, b_P \rangle_\rho$, where $z_P := \sum_{k=1}^K \widehat{z}_k \phi_k(\xi)$ and similarly for a_P, b_P with $\widehat{a}, \widehat{b} \in \mathbb{R}^K$. Using the fact that $(\mathcal{M}_k)_{\ell, m}$ is commutative in (k, m) a direct computation shows:

$$(2.8) \quad \mathcal{P}(\widehat{a}) = (\mathcal{M}_1 \widehat{a}, \mathcal{M}_2 \widehat{a}, \dots, \mathcal{M}_K \widehat{a}),$$

A useful lemma is given as follows.

Lemma 2.1. *For any two vectors $\widehat{a}, \widehat{b} \in \mathbb{R}^K$,*

$$(2.9) \quad \mathcal{P}(\widehat{a}) \widehat{b} = \mathcal{P}(\widehat{b}) \widehat{a}, \quad \widehat{b}^\top \mathcal{P}(\widehat{a}) = \widehat{a}^\top \mathcal{P}(\widehat{b}).$$

The proof is straightforward using (2.7) and (2.8) along with the symmetry of $\mathcal{P}(\cdot)$. This result is a ‘‘commutative’’ property of the operator $\mathcal{P}(\cdot)$. For example: For any $a, b, c \in \mathbb{R}^K$,

$$(2.10) \quad \frac{\partial}{\partial c} a^\top \mathcal{P}(c) b^\top = a^\top \mathcal{P}(b),$$

A *stochastic Galerkin* (SG) formulation of a ξ -parameterized PDE corresponds to making the ansatz that the state variable lies in the space P , and projecting the PDE residual onto the same space. Straightforward applications of this procedure to (nonlinear) hyperbolic PDEs typically do not result in hyperbolic SG formulations.

2.3. Hyperbolic-Preserving Stochastic Galerkin Formulation for Shallow Water Equation. In [9], we have derived a hyperbolicity-preserving stochastic Galerkin formulation for the shallow water equations. We briefly recall the results in this section. We make the ansatz that the solutions to h, q lie in the polynomial space P ,

$$(2.11a) \quad h \simeq h_P := \sum_{k=1}^K \hat{h}_k(x, t) \phi_k(\xi),$$

$$(2.11b) \quad q \simeq q_P := \sum_{k=1}^K (\hat{q})_k(x, t) \phi_k(\xi),$$

and use these to formulate a ξ -variable Galerkin projection of the SWE. We make a special choice of how the Galerkin projection of the nonlinear, non-polynomial term $(q)^2/h$ is truncated, which results in a *new* (stochastic Galerkin) system of balance laws whose state variables are the expansion coefficients in (2.11) [9]:

$$(2.12) \quad \hat{U}_t + (\hat{F}(\hat{U}))_x = \hat{S}(\hat{U}),$$

Here, $\hat{U} := (\hat{h}^\top, \hat{q}^\top)^\top \in \mathbb{R}^{2K}$, where \hat{h}, \hat{q} are each length- K vectors of the expansion coefficients in (2.11). The flux and the source terms are,

$$(2.13) \quad \hat{F}(\hat{U}) = \left(\mathcal{P}(\hat{q})\mathcal{P}^{-1}(\hat{h})\hat{q} + \frac{1}{2}g\mathcal{P}(\hat{h})\hat{h} \right), \quad \hat{S}(\hat{U}) = \begin{pmatrix} 0 \\ -g\mathcal{P}(\hat{h})\hat{B}_x \end{pmatrix},$$

cf. (1.2). The flux Jacobian, written in $K \times K$ blocks, is given by

$$(2.14) \quad \frac{\partial \hat{F}}{\partial \hat{U}} = \begin{pmatrix} O & I \\ g\mathcal{P}(\hat{h}) - \mathcal{P}(\hat{q})\mathcal{P}^{-1}(\hat{h})\mathcal{P}(\hat{u}) & \mathcal{P}(\hat{q})\mathcal{P}^{-1}(\hat{h}) + \mathcal{P}(\hat{u}) \end{pmatrix}.$$

We have introduced the term

$$(2.15) \quad \hat{u} = \mathcal{P}^{-1}(\hat{h})\hat{q},$$

which we view as the vector of the PCE coefficients of the x -velocity u introduced in (2.1), and is well-defined if $\mathcal{P}(\hat{h})$ is invertible.

The deterministic SWE are hyperbolic if the water height $h > 0$; there is a natural extension of this property to the SGSWE.

Theorem 2.1 (Theorem 3.1, [9]). *If the matrix $\mathcal{P}(\hat{h})$ is strictly positive definite for every point (x, t) in the computational spatial-temporal domain, then the SG formulation (2.12) is hyperbolic.*

This is proven by identifying a stochastic extension of the known eigenvector matrix for the deterministic SWE flux Jacobian $\frac{\partial F}{\partial U}$, and using this to show that $\frac{\partial \hat{F}}{\partial \hat{U}}$ is similar to a symmetric matrix and hence (2.12) is hyperbolic [9].

3. AN ENTROPY-ENTROPY FLUX PAIR FOR SGSWE SYSTEMS

The formulation (2.12) will be considered in what follows. Our goal will be to derive entropy-entropy flux pairs for these formulations. The first step is for us to recall a known entropy-entropy flux pair for the *deterministic* SWE system.

3.1. Entropy-Entropy Flux Pairs for Deterministic Shallow Water Equations. It is well-known that solutions to systems of conservation/balance laws can develop shock discontinuities in finite time for generic initial data. Therefore, weak solutions, i.e., solutions in the sense of distributions, are usually considered. However, weak solutions are not necessarily unique, and to mitigate this issue, an additional *entropy admissibility criteria* is imposed [8, 2] to identify the physically meaningful solution.

For a general balance law in one space dimension

$$(3.1) \quad U_t + F(U)_x = S(U),$$

its entropy-entropy flux pair $(E(U), H(U))$ satisfies a *companion* balance law

$$(3.2) \quad E(U)_t + H(U)_x = 0$$

where the *entropy* $E(U)$ is a scalar function that is convex in U , and H is an *entropy flux* function. In order to be consistent with the original balance law for smooth U , the entropy-entropy flux pair (E, H) should satisfy the following *compatibility condition*,

$$(3.3) \quad \frac{\partial E}{\partial U}(F_x - S) = H_x,$$

which is simply the condition ensuring that multiplying (3.1) by $\frac{\partial E}{\partial U}$ recovers (3.2) when solutions are smooth. In the case of $S \equiv 0$ and $(E, H) = (E(U), H(U))$, equation (3.3) is the usual entropy condition for conservation laws. For a general system of balance laws in several spatial dimensions, an entropy-entropy flux pair need not exist. However, for a hyperbolic system of balance laws emerging from continuum physics, the companion balance law (3.2) is usually related to the Second Law of thermodynamics, and the total energy of the system often serves as the entropy function. A variety of examples can be found in [8, Section 3.3]. For the *deterministic* SWE system in (1.1), the total energy [15] is

$$(3.4) \quad E^d(U) = \underbrace{\frac{1}{2}qu}_{\text{kinetic energy}} + \underbrace{\frac{1}{2}gh^2 + ghB}_{\text{potential energy}}.$$

where we recall that u is the velocity defined in (2.1). For any smooth solution U , a direct calculation yields,

$$(3.5) \quad E^d(U)_t + H^d(U)_x = 0,$$

where

$$(3.6) \quad H^d(U) = \frac{1}{2}qu^2 + gqh + gqB.$$

This, along with the fact that E^d is convex in U , establishes that (E^d, H^d) is a valid entropy-entropy flux pair for (1.1). For (weak) solutions with shocks, the entropy admissibility criteria is that energy should dissipate in accordance with a vanishing viscosity principle,

$$(3.7) \quad E^d(U)_t + H^d(U)_x \leq 0.$$

In what follows we will identify entropy-entropy flux pairs for the SGSWE model. This amounts to verifying that (i) such a pair satisfies the companion balance law (an equality for smooth solutions) and (ii) that the entropy function is convex in the state variable.

3.2. An Entropy-Entropy Flux Pair for the one-dimensional SGSWE. This section is dedicated to identifying an entropy-entropy flux pair for the SG system (2.12). In this section, we will return to the notation \widehat{U} (containing PC expansion coefficients) for the derivation of an entropy-entropy flux pair for the SG system. Our main result in this section is the following entropy-entropy flux pair for the one-dimensional SGSWE:

Theorem 3.1. *Define the function,*

$$(3.8a) \quad E(\widehat{U}) = \frac{1}{2} \left((\widehat{q})^\top \widehat{u} + g \|\widehat{h}\|^2 \right) + g \widehat{h}^\top \widehat{B},$$

and also the flux function,

$$(3.8b) \quad H(\widehat{U}) = \frac{1}{2} \widehat{u}^\top \mathcal{P}(\widehat{q}) \widehat{u} + g \widehat{q}^\top \widehat{h} + g \widehat{q}^\top \widehat{B},$$

If $\mathcal{P}(\widehat{h}) > 0$, then (E, H) is an entropy-entropy flux pair for the one-dimensional SGSWE (2.12).

Recall that \hat{u} above is defined in (2.15), and contains PC expansion coefficients for the velocity u defined in (2.1). In the absence of uncertainty, (3.8a) reduces to the deterministic total energy (3.4). The rest of this section is devoted to proving theorem 3.1, which amounts to showing that, if $\mathcal{P}(\hat{h}) > 0$, then E is convex in \hat{U} and (E, H) satisfy the companion balance law,

$$(3.9) \quad E(\hat{U})_t + H(\hat{U})_x = 0,$$

for smooth solutions \hat{U} . Note that for non-smooth solutions, (3.9) holds with $=$ replaced by \leq . We prove Theorem 3.1 with three intermediate results. Our first result is a technical condition that facilitates later computations.

Lemma 3.1 (Gradient of \hat{u}). *Let $\hat{q} \in \mathbb{R}^K$ be arbitrary, and let $\hat{h} \in \mathbb{R}^K$ be such that $\mathcal{P}(\hat{h})$ is invertible. Defining \hat{u} as in (2.15), then*

$$(3.10) \quad \frac{\partial \hat{u}}{\partial \hat{U}} = \left[\frac{\partial \hat{u}}{\partial \hat{h}}, \frac{\partial \hat{u}}{\partial \hat{q}} \right] = \left[-\mathcal{P}^{-1}(\hat{h})\mathcal{P}(\hat{u}), \mathcal{P}^{-1}(\hat{h}) \right]$$

Proof. If $A(t)$ is a t -parameterized matrix, then for any t at which A is invertible,

$$\frac{\partial}{\partial t} A^{-1}(t) = -A^{-1}(t) \frac{\partial A(t)}{\partial t} A^{-1}(t).$$

Applying this to \mathcal{P} , we have,

$$(3.11) \quad \frac{\partial \mathcal{P}^{-1}(\hat{h})}{\partial \hat{h}_\ell} = -\mathcal{P}^{-1}(\hat{h}) \frac{\partial \mathcal{P}(\hat{h})}{\partial \hat{h}_\ell} \mathcal{P}^{-1}(\hat{h}) \stackrel{(2.8)}{=} -\mathcal{P}^{-1}(\hat{h}) \mathcal{M}_\ell \mathcal{P}^{-1}(\hat{h}),$$

and hence,

$$(3.12) \quad \frac{\partial \hat{u}}{\partial \hat{h}_\ell} = \frac{\partial \mathcal{P}^{-1}(\hat{h})}{\partial \hat{h}_\ell} \hat{q} \stackrel{(3.11)}{=} -\mathcal{P}^{-1}(\hat{h}) \mathcal{M}_\ell \mathcal{P}^{-1}(\hat{h}) \hat{q} \stackrel{(2.15)}{=} \mathcal{P}^{-1}(\hat{h}) \mathcal{M}_\ell \hat{u}.$$

Therefore,

$$(3.13) \quad \frac{\partial \hat{u}}{\partial \hat{h}} = \left[-\mathcal{P}^{-1}(\hat{h}) \mathcal{M}_1 \hat{u}, \dots, -\mathcal{P}^{-1}(\hat{h}) \mathcal{M}_K \hat{u} \right] \stackrel{(2.8)}{=} -\mathcal{P}^{-1}(\hat{h}) \mathcal{P}(\hat{u}),$$

proving the desired relation for $\frac{\partial \hat{u}}{\partial \hat{h}}$. The relation for $\frac{\partial \hat{u}}{\partial \hat{q}}$ is immediate from the definition (2.15). \square

Lemma 3.2 (Convexity of $E(\hat{U})$). *If $\mathcal{P}(\hat{h})$ is positive definite, then the function $E(\hat{U})$ defined in (3.8a) is convex in \hat{U} .*

Proof. Using the definition (2.15) of \hat{u} , note that,

$$(3.14) \quad E(\hat{U}) = \underbrace{\frac{1}{2}(\hat{q})^\top \mathcal{P}^{-1}(\hat{h}) \hat{q}}_{f_1(\hat{U})} + \underbrace{\frac{g}{2} \hat{h}^\top \hat{h} + g \hat{h}^\top \hat{B}}_{f_2(\hat{U})},$$

and therefore in particular,

$$(3.15) \quad \frac{\partial^2 E}{\partial \hat{U}^2} = \frac{\partial^2 f_1}{\partial \hat{U}^2} + \frac{\partial^2 f_2}{\partial \hat{U}^2}.$$

We will show that this Hessian is positive definite. Clearly we have,

$$(3.16) \quad \frac{\partial f_2}{\partial \hat{U}} = (g \hat{h}^\top + g \hat{B}^\top, 0) \in \mathbb{R}^{1 \times 2K}, \quad \frac{\partial^2 f_2}{\partial \hat{U}^2} = \begin{pmatrix} gI & 0 \\ 0 & 0 \end{pmatrix} \in \mathbb{R}^{2K \times 2K}.$$

Using the previous lemma, we can directly compute,

$$(3.17) \quad \frac{\partial f_1}{\partial \hat{h}} = \frac{1}{2}(\hat{q})^\top \frac{\partial \hat{u}}{\partial \hat{h}} \stackrel{(3.10), (2.15)}{=} -\frac{1}{2} \hat{u}^\top \mathcal{P}(\hat{u}), \quad \frac{\partial f_1}{\partial \hat{q}} = (\hat{q})^\top \mathcal{P}^{-1}(\hat{h}) = \hat{u}^\top,$$

which in turn implies,

$$\frac{\partial^2 f_1}{\partial \hat{q}^2} = \mathcal{P}^{-1}(\hat{h}), \quad \frac{\partial^2 f_1}{\partial \hat{h} \partial \hat{q}} \stackrel{(3.10)}{=} \left(-\mathcal{P}^{-1}(\hat{h}) \mathcal{P}(\hat{u}) \right)^\top = -\mathcal{P}(\hat{u}) \mathcal{P}^{-1}(\hat{h}),$$

and finally,

$$\frac{\partial^2 f_1}{\partial \hat{h}^2} = \frac{1}{2} \frac{\partial}{\partial \hat{h}} \left(-\hat{u}^\top \mathcal{P}(\hat{u}) \right) \stackrel{(3.10)}{=} \mathcal{P}(\hat{u}) \mathcal{P}^{-1}(\hat{h}) \mathcal{P}(\hat{u})$$

Hence, the Hessian of f_1 is,

$$\frac{\partial^2 f_1}{\partial \hat{U}^2} = \begin{pmatrix} \mathcal{P}(\hat{u}) \mathcal{P}^{-1}(\hat{h}) \mathcal{P}(\hat{u}) & -\mathcal{P}(\hat{u}) \mathcal{P}^{-1}(\hat{h}) \\ -\mathcal{P}^{-1}(\hat{h}) \mathcal{P}(\hat{u}) & \mathcal{P}^{-1}(\hat{h}) \end{pmatrix}.$$

A direct computation of the quadratic form associated to this Hessian using an arbitrary vector $(w_1^\top, w_2^\top)^\top \in \mathbb{R}^{2K}$ yields,

$$(w_1^\top, w_2^\top) \frac{\partial^2 f_1}{\partial \hat{U}^2} \begin{pmatrix} w_1 \\ w_2 \end{pmatrix} = (\mathcal{P}(\hat{u})w_1 - w_2)^\top \mathcal{P}^{-1}(\hat{h}) (\mathcal{P}(\hat{u})w_1 - w_2) \geq 0.$$

Finally, combining the above with (3.15) and (3.16) yields,

$$(w_1^\top, w_2^\top) \frac{\partial^2 E}{\partial \hat{U}^2} \begin{pmatrix} w_1 \\ w_2 \end{pmatrix} = g \|w_1\|^2 + (\mathcal{P}(\hat{u})w_1 - w_2)^\top \mathcal{P}^{-1}(\hat{h}) (\mathcal{P}(\hat{u})w_1 - w_2),$$

which is non-negative since $\mathcal{P}(\hat{h})$ is positive-definite. Therefore, E is convex, as desired. In addition, since the above expression vanishes if and only if $w_1 = w_2 = 0$, then E is also strictly convex. \square

The final piece needed to prove Theorem 3.1 is to establish that the entropy function E along with the flux function H defined in (3.8b) satisfy the companion balance law.

Lemma 3.3 ((E, H) satisfy the companion balance law). *When U is a smooth function, the pair (E, H) defined in (3.8) satisfies*

$$(3.18) \quad E(\hat{U})_t + H(\hat{U})_x = 0.$$

Proof. The compatibility condition we seek to show, equivalent to (3.18), is,

$$(3.19) \quad \frac{\partial E}{\partial \hat{U}} \left(\frac{\partial \hat{F}}{\partial \hat{U}} \frac{\partial \hat{U}}{\partial x} - \hat{S} \right) = \frac{\partial H}{\partial x},$$

cf. (3.3). To proceed we split both entropy functions into two pieces:

$$(3.20a) \quad E(\hat{U}) = E_1(\hat{U}) + E_2(\hat{U}), \quad E_1(\hat{U}) := \frac{1}{2} \left((\hat{q})^\top \hat{u} + g \|\hat{h}\|^2 \right), \quad E_2(\hat{U}) := \hat{g} \hat{h}^\top \hat{B},$$

$$(3.20b) \quad H(\hat{U}) = H_1(\hat{U}) + H_2(\hat{U}), \quad H_1(\hat{U}) := \frac{1}{2} \hat{u}^\top \mathcal{P}(\hat{q}) \hat{u} + g(\hat{q})^\top \hat{h}, \quad H_2(\hat{U}) = g(\hat{q})^\top \hat{B}$$

From (3.14), (3.16), and (3.17), we have already computed the gradient of E :

$$(3.21) \quad \frac{\partial E_1}{\partial \hat{U}} = \left(-\frac{1}{2} \hat{u}^\top \mathcal{P}(\hat{u}) + \hat{g} \hat{h}^\top, \hat{u}^\top \right), \quad \frac{\partial E_2}{\partial \hat{U}} = \left(g \hat{B}^\top, 0 \right).$$

Combining these expressions with the flux Jacobian in (2.14) and the source term in (2.13) yields,

$$(3.22a) \quad -\frac{\partial E_1}{\partial \hat{U}} \hat{S} + \frac{\partial E_2}{\partial \hat{U}} \left(\frac{\partial \hat{F}}{\partial \hat{U}} \frac{\partial \hat{U}}{\partial x} - \hat{S} \right) = g \hat{B}^\top \frac{\partial \hat{q}}{\partial x} + \hat{g} \hat{q}^\top \hat{B}_x \stackrel{(3.20b)}{=} \frac{\partial H_2}{\partial x}$$

Note then that if we are able to show,

$$(3.22b) \quad \frac{\partial E_1}{\partial \hat{U}} \frac{\partial \hat{F}}{\partial \hat{U}} = \frac{\partial H_1}{\partial \hat{U}},$$

then the expressions (3.22) are equivalent to (3.19). Therefore, we are left only to show (3.22b). A direct computation with (3.21) and (2.14) yields,

$$\frac{\partial E_1}{\partial \widehat{U}} \frac{\partial \widehat{F}}{\partial \widehat{U}} = \left(g(\widehat{q})^\top - \widehat{u}^\top \mathcal{P}(\widehat{q}) \mathcal{P}^{-1}(\widehat{h}) \mathcal{P}(\widehat{u}), \quad \widehat{g} \widehat{h}^\top + \frac{1}{2} \widehat{u}^\top \mathcal{P}(\widehat{u}) + \widehat{u}^\top \mathcal{P}(\widehat{q}) \mathcal{P}^{-1}(\widehat{h}) \right)$$

On the other hand, we have the expressions,

$$\begin{aligned} \frac{\partial}{\partial \widehat{h}} \frac{1}{2} \widehat{u}^\top \mathcal{P}(\widehat{q}) \widehat{u} &= \widehat{u}^\top \mathcal{P}(\widehat{q}) \frac{\partial \widehat{u}}{\partial \widehat{h}} \stackrel{(3.10)}{=} -\widehat{u}^\top \mathcal{P}(\widehat{q}) \mathcal{P}^{-1}(\widehat{h}) \mathcal{P}(\widehat{u}), \\ \frac{\partial}{\partial \widehat{q}} \frac{1}{2} \widehat{u}^\top \mathcal{P}(\widehat{q}) \widehat{u} &= \widehat{u}^\top \mathcal{P}(\widehat{q}) \frac{\partial \widehat{u}}{\partial \widehat{q}} + \frac{1}{2} \left(\frac{\partial}{\partial \widehat{q}} z^\top \mathcal{P}(\widehat{q}) z \right) \Big|_{z \leftarrow \widehat{u}} \stackrel{(2.10), (3.10)}{=} \widehat{u}^\top \mathcal{P}(\widehat{q}) \mathcal{P}^{-1}(\widehat{h}) + \frac{1}{2} \widehat{u}^\top \mathcal{P}(\widehat{u}) \end{aligned}$$

and using these to compute $\frac{\partial H_1}{\partial \widehat{U}}$ shows that (3.22b) is true, completing the proof. \square

The proof of Theorem 3.1 is complete: Lemmas (3.2) and (3.3) imply that (E, H) as defined in (3.8) are an entropy-entropy flux pair for (2.12).

Remark 3.1. *The quantities,*

$$(3.23) \quad \widehat{V} := \left(\frac{\partial E}{\partial \widehat{U}} \right)^\top = \left(-\frac{1}{2} \widehat{u}^\top \mathcal{P}(\widehat{u}) + g(\widehat{h} + \widehat{B})^\top, \widehat{u}^\top \right)^\top, \quad \Psi := \widehat{V} \widehat{F} - H \stackrel{(2.15), (3.8b)}{=} \frac{1}{2} g \widehat{u}^\top \mathcal{P}(\widehat{h}) \widehat{h},$$

are called the entropy variable and stochastic energy potential, respectively. These variables serve important roles in the construction of the energy conservative and the energy stable schemes that we develop later.

4. WELL-BALANCED ENERGY CONSERVATIVE AND ENERGY STABLE SCHEMES FOR SG 1D SWE

In this section, we present several well-balanced energy conservative and energy stable numerical scheme for SG SWE. The schemes designed below are stochastic extensions of the schemes developed in [15]. Our entropy-entropy flux pairs developed in Section 3 will be crucial ingredients for energy conservative and energy stable schemes for the SG formulation (2.12)-(2.15).

We also need to specify the well-balanced property we are interested in: By “well-balanced”, we mean that the scheme can preserve the stochastic “lake-at-rest” state exactly at the discrete level.

Definition 4.1 (Well-Balanced SGSWE Property, [9]). *We say that a solution (h_P, q_P) to (2.12) is well-balanced if it satisfies the stochastic “lake-at-rest” solution,*

$$(4.1) \quad q_P(x, t, \xi) \equiv 0, \quad h_P(x, t, \xi) + \Pi_P[B](x, t, \xi) \equiv C(\xi),$$

where $C(\xi)$ is a random scalar depending only on ξ , Π_P corresponds to a polynomial truncation, cf. (2.5), and subscripts P refer to the (stochastic) discrete solution on the subspace P . In terms of our previous notation for P -expansion coefficients, equation (4.1) is equivalent to the following vector equation

$$(4.2) \quad \widehat{q} \equiv \mathbf{0}, \quad \widehat{h} + \widehat{B} \equiv \widehat{C}, \quad \forall (x, t) \in \mathcal{D} \times [0, T],$$

where \mathcal{D} is the spatial domain and T is the terminal time.

We emphasize that even without introducing the lake-at-rest definition (4.1), the vector equation (4.2) itself is a steady state of the SG system (2.12).

4.1. Energy Conservative Schemes. We consider the semi-discrete form for FV schemes for (2.12) over a uniform mesh in the x variable:

$$(4.3) \quad \frac{d}{dt} \mathbf{U}_i = -\frac{\mathcal{F}_{i+\frac{1}{2}} - \mathcal{F}_{i-\frac{1}{2}}}{\Delta x} + \mathbf{S}_i.$$

Here, $\mathbf{U}_i \approx \frac{1}{\Delta x} \int_{\mathcal{I}_i} \widehat{U}(x, t) dx$ is the approximation of the cell averages of \widehat{U} over cells $\mathcal{I}_i := [x_{i-1/2}, x_{i+1/2}]$ at time t , and $\Delta x = |\mathcal{I}_i| = x_{i+1/2} - x_{i-1/2}$. The terms $\mathcal{F}_{i\pm 1/2}$ are numerical fluxes at the boundaries of the cells, which are functions of neighboring states, e.g., $\mathcal{F}_{i+1/2}$ is a function of \mathbf{U}_i and \mathbf{U}_{i+1} . The term $\mathbf{S}_i \approx \frac{1}{\Delta x} \int_{\mathcal{I}_i} \widehat{S}(\widehat{U}, \widehat{B}) dx$ is a discretization of the source term, which we will design below to be well-balanced. To reiterate our notation: normal typeset capital letters (sometimes with “hat” notation) refers to degrees of freedom associated to discretizing *only* the stochastic variable ξ , i.e., $(\widehat{U}, \widehat{h}, \widehat{q}, \widehat{B})$. Boldface notation with subscripts i refers to degrees of freedom associated to a subsequent discretization of the spatial variable x over cell \mathcal{I}_i , i.e., $(\mathbf{U}_i, \mathbf{h}_i, \mathbf{q}_i, \mathbf{B}_i)$. We define the discrete velocity variable \mathbf{u}_i in a manner analogous to (2.15):

$$(4.4) \quad \mathbf{u}_i := \mathcal{P}(\mathbf{h}_i)^{-1} \mathbf{q}_i.$$

Discrete entropic quantities are derived from the discrete conservative variables \mathbf{U}_i and velocity variable \mathbf{u}_i . I.e., the following are direct generalizations of the definition of $E(\widehat{U})$ in (3.8a), and of (\widehat{V}, Ψ) in (3.23):

$$(4.5a) \quad \mathbf{E}_i := \frac{1}{2} (\mathbf{q}_i^\top \mathbf{u}_i + g \|\mathbf{h}_i\|^2) + g \mathbf{h}_i^\top \mathbf{B}_i,$$

$$(4.5b) \quad \mathbf{V}_i := \left(\frac{\partial \mathbf{E}_i}{\partial \mathbf{U}_i} \right)^\top = \left(-\frac{1}{2} \mathbf{u}_i^\top \mathcal{P}(\mathbf{u}_i) + g(\mathbf{h}_i + \mathbf{B}_i)^\top, \mathbf{u}_i^\top \right)^\top,$$

$$(4.5c) \quad \Psi_i := \mathbf{V}_i \widehat{F}(\mathbf{U}_i) - H(\mathbf{U}_i) = \frac{1}{2} g \mathbf{u}_i^\top \mathcal{P}(\mathbf{h}_i) \mathbf{h}_i$$

We now introduce some notation that is used in [15] for averages and jumps at cell interfaces:

$$(4.6) \quad \bar{\mathbf{a}}_{i+1/2} := \frac{1}{2} (\mathbf{a}_{i+1} + \mathbf{a}_i), \quad \llbracket \mathbf{a} \rrbracket_{i+1/2} := \mathbf{a}_{i+1} - \mathbf{a}_i,$$

where \mathbf{a}_i is the cell average over \mathcal{I}_i . The expressions above are equivalent to,

$$(4.7) \quad \mathbf{a}_i = \bar{\mathbf{a}}_{i+1/2} - \frac{\llbracket \mathbf{a} \rrbracket_{i+1/2}}{2} = \bar{\mathbf{a}}_{i-1/2} + \frac{\llbracket \mathbf{a} \rrbracket_{i-1/2}}{2},$$

and all these expressions are valid regardless of the size of \mathbf{a} (e.g., both row and column vectors are allowed). We will require some additional technical results for interfacial averages and jumps.

Lemma 4.1. *Let $\mathbf{a}_i, \mathbf{b}_i$ be any spatially discrete quantities. Then:*

$$(4.8a) \quad \mathcal{P}(\bar{\mathbf{a}}_{i+\frac{i}{2}}) \llbracket \mathbf{a} \rrbracket_{i+\frac{i}{2}} = \frac{1}{2} \llbracket \mathcal{P}(\mathbf{a}) \mathbf{a} \rrbracket_{i+\frac{i}{2}}.$$

$$(4.8b) \quad \llbracket \mathbf{a} \rrbracket_{i+\frac{i}{2}}^\top \bar{\mathbf{b}}_{i+\frac{i}{2}} + \llbracket \mathbf{b} \rrbracket_{i+\frac{i}{2}}^\top \bar{\mathbf{a}}_{i+\frac{i}{2}} = \llbracket \mathbf{a}^\top \mathbf{b} \rrbracket_{i+\frac{i}{2}}$$

Proof. Due to linearity of \mathcal{P} , then,

$$\mathcal{P}(\bar{\mathbf{a}}_{i+\frac{i}{2}}) \llbracket \mathbf{a} \rrbracket_{i+\frac{i}{2}} \stackrel{(2.7)}{=} \mathcal{P} \left(\frac{1}{2} (\mathbf{a}_{i+1} + \mathbf{a}_i) \right) (\mathbf{a}_{i+1} - \mathbf{a}_i) \stackrel{(2.9)}{=} \frac{1}{2} (\mathcal{P}(\mathbf{a}_{i+1}) \mathbf{a}_{i+1} - \mathcal{P}(\mathbf{a}_i) \mathbf{a}_i) = \frac{1}{2} \llbracket \mathcal{P}(\mathbf{a}) \mathbf{a} \rrbracket_{i+\frac{i}{2}},$$

which proves (4.8a). Similarly, (4.8b) can be proven directly:

$$\begin{aligned} \llbracket \mathbf{a} \rrbracket_{i+\frac{i}{2}}^\top \bar{\mathbf{b}}_{i+\frac{i}{2}} + \llbracket \mathbf{b} \rrbracket_{i+\frac{i}{2}}^\top \bar{\mathbf{a}}_{i+\frac{i}{2}} &= \frac{1}{2} \left((\mathbf{a}_{i+1} - \mathbf{a}_i)^\top (\mathbf{b}_{i+1} + \mathbf{b}_i) + (\mathbf{b}_{i+1} - \mathbf{b}_i)^\top (\mathbf{a}_{i+1} + \mathbf{a}_i) \right) \\ &= \mathbf{a}_{i+1}^\top \mathbf{b}_{i+1} - \mathbf{a}_i^\top \mathbf{b}_i = \llbracket \mathbf{a}^\top \mathbf{b} \rrbracket_{i+\frac{i}{2}}. \end{aligned}$$

□

We now make particular definitions for energy conservative and energy stable schemes for one-dimensional systems of balance laws. To provide context, with no source terms (i.e. $\mathbf{S}_i = 0$) then spatial discretizations of the form (4.3) are called *conservative* schemes since they imply,

$$(4.9) \quad \frac{d}{dt} \sum_{i \in [M]} \Delta x \mathbf{U}_i(t) = [\mathcal{F}_{1/2} - \mathcal{F}_{M+1/2}], \quad (\text{vanishing source, } \mathbf{S}_i = 0),$$

and in particular with periodic boundary conditions, then this implies that the cumulative amount of \widehat{U} in the system is constant in time.¹

To translate this concept to the notion of an energy conservative scheme, note that an entropy-entropy flux pair (E, H) introduced in section 3 is explicitly a function of the state \widehat{U} and inputs in the source term (here, \widehat{B}). Hence, the semi-discrete form (4.3) can be transformed into a semi-discrete form for the companion balance law (3.9). Then we call (4.3) energy conservative if it implies a conservative scheme for the companion balance law that describes the evolution of the entropy (energy).

Definition 4.2 (Energy conservative and energy stable schemes). *Suppose that the system of balance laws (2.12) has an entropy-entropy flux pair (E, H) where $E(\widehat{U})$ can be interpreted as energy for the system. Then the semi-discrete FV scheme (4.3) is an Energy Conservative (EC) scheme if it can be rewritten as the following semi-discrete form for the evolution of the numerical cell averages \mathbf{E}_i of E :*

$$(4.10) \quad \frac{d}{dt} \mathbf{E}_i(t) = -\frac{1}{\Delta x} (\mathcal{H}_{i+1/2} - \mathcal{H}_{i-1/2}), \quad i \in [M],$$

where $\mathcal{H}_{i+1/2}$ is some numerical entropy flux at the interface location $x = x_{i+1/2}$. The scheme (4.3) is called an Energy Stable (ES) scheme if

$$(4.11) \quad \frac{d}{dt} \mathbf{E}_i(t) \leq -\frac{1}{\Delta x} (\mathcal{H}_{i+1/2} - \mathcal{H}_{i-1/2}), \quad i \in [M].$$

Note that the definitions above are cell-wise conditions that are stronger than a global condition such as (4.9).

4.2. An EC scheme for the SGSWE. In this section we present an EC scheme for the one-dimensional SGSWE system (2.12). We use the conservative scheme (4.3), with the following choices of flux and source terms:

$$(4.12a) \quad \mathcal{F}_{i+1/2} = \mathcal{F}_{i+1/2}^{\text{EC}} := \left(\begin{array}{c} \mathcal{P}(\overline{\mathbf{h}}_{i+\frac{1}{2}}) \overline{\mathbf{u}}_{i+\frac{1}{2}} \\ \frac{g}{2} (\overline{\mathcal{P}(\mathbf{h})\mathbf{h}})_{i+\frac{1}{2}} + \mathcal{P}(\overline{\mathbf{u}}_{i+\frac{1}{2}}) \mathcal{P}(\overline{\mathbf{h}}_{i+\frac{1}{2}}) \overline{\mathbf{u}}_{i+\frac{1}{2}} \end{array} \right),$$

$$(4.12b) \quad \mathbf{S}_i = \left(\begin{array}{c} \mathbf{0} \\ -\frac{g}{2\Delta x} (\mathcal{P}(\overline{\mathbf{h}}_{i+\frac{1}{2}}) \llbracket \mathbf{B} \rrbracket_{i+\frac{1}{2}} + \mathcal{P}(\overline{\mathbf{h}}_{i-\frac{1}{2}}) \llbracket \mathbf{B} \rrbracket_{i-\frac{1}{2}}) \cdot \end{array} \right)$$

Above, the interfacial averages $\overline{\mathbf{u}}_{i+1/2}$ are computed as defined in (4.6). Our main result for this scheme is as follows.

Theorem 4.1 (EC Scheme). *Suppose the bottom topography function B is independent of time. Consider the semi-discrete scheme (4.3) for the SGSWE system (2.12). Suppose that the flux and source terms are selected as in (4.12). Then, this is a well-balanced EC scheme with local truncation error $\mathcal{O}(\Delta x^2)$.*

The remainder of this section is devoted to the proof, which requires some intermediate steps. First, we show that \mathbf{S}_i is a well-balanced choice for the source term discretization.

¹For non-periodic boundary conditions, the energy would increase/decrease depending on the boundary conditions and their corresponding impact on the boundary fluxes.

Lemma 4.2. *Suppose \mathbf{S}_i is chosen as in (4.12b). If the bottom topography B is independent of time, then (4.3) is a well-balanced scheme in the sense of definition 4.1.*

Proof. Given initial data

$$(4.13) \quad \mathbf{u}_i \equiv \mathbf{0}, \quad \mathbf{h}_i + \mathbf{B}_i = \text{const vector}, \quad \forall i,$$

the well-balanced property with time-independent bottom topography (see definition 4.1) requires that, for every i ,

$$(4.14) \quad \frac{d}{dt} \mathbf{h}_i \equiv 0, \quad \frac{d}{dt} \mathbf{q}_i \equiv 0.$$

We first notice that,

$$(4.15) \quad \begin{aligned} \left(\overline{\mathcal{P}(\mathbf{h})\mathbf{h}} \right)_{i+\frac{1}{2}} - \left(\overline{\mathcal{P}(\mathbf{h})\mathbf{h}} \right)_{i-\frac{1}{2}} &= \frac{1}{2} \left(\llbracket \mathcal{P}(\mathbf{h})\mathbf{h} \rrbracket_{i+\frac{1}{2}} + \llbracket \mathcal{P}(\mathbf{h})\mathbf{h} \rrbracket_{i-\frac{1}{2}} \right) \\ &\stackrel{(4.8a)}{=} \mathcal{P}(\bar{\mathbf{h}}_{i+\frac{1}{2}}) \llbracket \mathbf{h} \rrbracket_{i+\frac{1}{2}} + \mathcal{P}(\bar{\mathbf{h}}_{i-\frac{1}{2}}) \llbracket \mathbf{h} \rrbracket_{i-\frac{1}{2}}. \end{aligned}$$

Note that with initialization (4.13), then $\mathbf{u}_i = 0$, and hence $\bar{\mathbf{u}}_{i+1/2} = 0$. Therefore the semi-discrete scheme (4.3) with the flux and source terms in (4.12) yields,

$$(4.16) \quad \begin{aligned} \frac{d}{dt} \mathbf{h}_i &= -\frac{1}{\Delta x} \left(\mathcal{P}(\bar{\mathbf{h}}_{i+\frac{1}{2}}) \bar{\mathbf{u}}_{i+\frac{1}{2}} - \mathcal{P}(\bar{\mathbf{h}}_{i-\frac{1}{2}}) \bar{\mathbf{u}}_{i-\frac{1}{2}} \right) = \mathbf{0}, \\ \frac{d}{dt} \mathbf{q}_i &= -\frac{g}{2\Delta x} \left(\left(\overline{\mathcal{P}(\mathbf{h})\mathbf{h}} \right)_{i+\frac{1}{2}} - \left(\overline{\mathcal{P}(\mathbf{h})\mathbf{h}} \right)_{i-\frac{1}{2}} \right) \\ &\quad - \frac{g}{2\Delta x} \left(\mathcal{P}(\bar{\mathbf{h}}_{i+\frac{1}{2}}) \llbracket \mathbf{B} \rrbracket_{i+\frac{1}{2}} + \mathcal{P}(\bar{\mathbf{h}}_{i-\frac{1}{2}}) \llbracket \mathbf{B} \rrbracket_{i-\frac{1}{2}} \right) \\ &\stackrel{(4.15)}{=} -\frac{g}{2\Delta x} \left(\mathcal{P}(\bar{\mathbf{h}}_{i+\frac{1}{2}}) \llbracket \mathbf{h} + \mathbf{B} \rrbracket_{i+\frac{1}{2}} + \mathcal{P}(\bar{\mathbf{h}}_{i-\frac{1}{2}}) \llbracket \mathbf{h} + \mathbf{B} \rrbracket_{i-\frac{1}{2}} \right) \stackrel{(4.13)}{=} \mathbf{0}, \end{aligned}$$

which establishes (4.14). \square

Lemma 4.3. *The flux and source terms in (4.12) commit a local truncation error of $\mathcal{O}(\Delta x^2)$.*

The proof is direct, by assuming $(\mathbf{U}_i, \mathbf{B}_i)$ are exact cell averages of spatially smooth functions (\hat{U}, \hat{B}) and then comparing $\mathcal{F}_{i+1/2}$ and \mathbf{S}_i to $\hat{F}(\hat{U})|_{x=x_{i+1/2}}$ and $\hat{S}(\hat{U})|_{x=x_i}$, respectively, where \hat{F} and \hat{S} are the exact flux and source functions in (2.13). Therefore we omit most details, pointing out only the following quantitative approximations in space (ignoring the time variable t):

$$\begin{aligned} \bar{\mathbf{U}}_{i+1/2} &= \hat{U}(x_{i+1/2}) + \mathcal{O}(\Delta x^2), & \llbracket \mathbf{U} \rrbracket_{i+1/2} &= \Delta x \hat{U}_x(x_{i+1/2}) + \mathcal{O}(\Delta x^2) \\ \mathcal{P}(\bar{\mathbf{h}}_{i+1/2}) &= \mathcal{P}(\hat{h}(x_{i+1/2})) + \mathcal{O}(\Delta x^2), & \bar{\mathbf{u}}_{i+1/2} &= \hat{u}(x_{i+1/2}) + \mathcal{O}(\Delta x^2). \end{aligned}$$

Note that the implicit constants hidden in the asymptotic notation above depend on the maximum singular value of $\mathcal{P}(\hat{h}_{xx}(x))$ and the minimum singular value of $\mathcal{P}(\hat{h}(x_{i+1/2}))$.

The final result we need is a sufficient condition for a numerical flux to result in an EC scheme.

Lemma 4.4. *Let \mathbf{S}_i be chosen as in (4.12b). Suppose that $\mathcal{F}_{i+1/2}$ satisfies*

$$(4.17) \quad \llbracket \mathbf{V} \rrbracket_{i+\frac{1}{2}}^\top \mathcal{F}_{i+\frac{1}{2}} = \llbracket \Psi \rrbracket_{i+\frac{1}{2}} + g \llbracket \mathbf{B} \rrbracket_{i+\frac{1}{2}}^\top \mathcal{P}(\bar{\mathbf{h}}_{i+\frac{1}{2}}) \bar{\mathbf{u}}_{i+\frac{1}{2}}.$$

Then the corresponding FV scheme (4.3) is an EC scheme, i.e., satisfies (4.10), where the numerical energy flux is given by,

$$(4.18) \quad \mathcal{H}_{i+\frac{1}{2}} := \bar{\mathbf{V}}_{i+\frac{1}{2}}^\top \mathcal{F}_{i+\frac{1}{2}} - \bar{\Psi}_{i+\frac{1}{2}} - \frac{g}{4} \llbracket \mathbf{B} \rrbracket_{i+\frac{1}{2}}^\top \mathcal{P}(\bar{\mathbf{h}}_{i+\frac{1}{2}}) \llbracket \mathbf{u} \rrbracket_{i+\frac{1}{2}}.$$

Proof. Multiplying (4.3) by \mathbf{V}_i^\top and using the definition of \mathbf{V}_i in (4.5b), we obtain,

$$(4.19) \quad \frac{d}{dt} \mathbf{E}_i = -\frac{1}{\Delta x} \left(\underbrace{\mathbf{V}_i^\top \mathcal{F}_{i+\frac{1}{2}}}_{(A1)} - \underbrace{\mathbf{V}_i^\top \mathcal{F}_{i-\frac{1}{2}}}_{(A2)} - \underbrace{\Delta x \mathbf{V}_i^\top \bar{\mathbf{S}}_i}_{(B)} \right)$$

The first term, labeled (A1), can be expanded to,

$$\begin{aligned}
\text{(A1)} &\stackrel{(4.7)}{=} \bar{\mathbf{V}}_{i+1/2}^\top \mathcal{F}_{i+1/2} - \frac{1}{2} \llbracket \mathbf{V} \rrbracket_{i+1/2}^\top \mathcal{F}_{i+1/2} \\
&\stackrel{(4.17)(4.18)}{=} \mathcal{H}_{i+\frac{1}{2}} + \bar{\Psi}_{i+\frac{1}{2}} + \frac{g}{4} \llbracket \mathbf{B} \rrbracket_{i+\frac{1}{2}}^\top \mathcal{P}(\bar{\mathbf{h}}_{i+\frac{1}{2}}) \llbracket \mathbf{u} \rrbracket_{i+\frac{1}{2}} - \frac{1}{2} \llbracket \Psi \rrbracket_{i+\frac{1}{2}} - \frac{g}{2} \llbracket \mathbf{B} \rrbracket_{i+\frac{1}{2}}^\top \mathcal{P}(\bar{\mathbf{h}}_{i+\frac{1}{2}}) \bar{\mathbf{u}}_{i+\frac{1}{2}} \\
&\stackrel{(4.7)}{=} \mathcal{H}_{i+\frac{1}{2}} + \Psi_i - \frac{g}{2} \llbracket \mathbf{B} \rrbracket_{i+\frac{1}{2}}^\top \mathcal{P}(\bar{\mathbf{h}}_{i+\frac{1}{2}}) \mathbf{u}_i
\end{aligned}$$

In an analogous computation, the term labeled (A2) is given by,

$$\text{(A2)} = \mathcal{H}_{i-\frac{1}{2}} + \Psi_i + \frac{g}{2} \llbracket \mathbf{B} \rrbracket_{i-\frac{1}{2}}^\top \mathcal{P}(\bar{\mathbf{h}}_{i-\frac{1}{2}}) \mathbf{u}_i$$

Finally, a direct computation shows that term (B) is,

$$\text{(B)} \stackrel{(4.12b),(4.5b)}{=} -\frac{g}{2} \mathbf{u}_i^\top \mathcal{P}(\bar{\mathbf{h}}_{i+\frac{1}{2}}) \llbracket \mathbf{B} \rrbracket_{i+\frac{1}{2}} - \frac{g}{2} \mathbf{u}_i^\top \mathcal{P}(\bar{\mathbf{h}}_{i-\frac{1}{2}}) \llbracket \mathbf{B} \rrbracket_{i-\frac{1}{2}}$$

Using the expressions for terms (A1), (A2), and (B) derived above in (4.19) establishes that the scheme satisfies (4.10), i.e., is an EC scheme. \square

We now have all the ingredients necessary to prove theorem 4.1.

Proof of theorem 4.1. Lemmas 4.2 and 4.3 verify that the scheme is well-balanced and second-order. We therefore need only show that it is EC. To do this, we must verify the condition in lemma 4.4. We accomplish this with direct computation:

$$\begin{aligned}
&\llbracket \mathbf{V} \rrbracket_{i+\frac{1}{2}}^\top \mathcal{F}_{i+\frac{1}{2}}^{\text{EC}} \stackrel{(4.5b),(4.12a)}{=} \left(g \left(\llbracket \mathbf{h} \rrbracket_{i+\frac{1}{2}} + \llbracket \mathbf{B} \rrbracket_{i+\frac{1}{2}} \right) - \frac{1}{2} \llbracket \mathcal{P}(\mathbf{u}) \mathbf{u} \rrbracket_{i+\frac{1}{2}} \right)^\top \mathcal{P}(\bar{\mathbf{h}}_{i+\frac{1}{2}}) \bar{\mathbf{u}}_{i+\frac{1}{2}} \\
&\quad + \llbracket \mathbf{u} \rrbracket_{i+\frac{1}{2}}^\top \left(\frac{g}{2} \left(\overline{\mathcal{P}(\mathbf{h}) \mathbf{h}} \right)_{i+\frac{1}{2}} + \mathcal{P}(\bar{\mathbf{u}}_{i+\frac{1}{2}}) \mathcal{P}(\bar{\mathbf{h}}_{i+\frac{1}{2}}) \bar{\mathbf{u}}_{i+\frac{1}{2}} \right) \\
&\stackrel{(4.8a)}{=} g \left(\llbracket \mathbf{h} \rrbracket_{i+\frac{1}{2}} + \llbracket \mathbf{B} \rrbracket_{i+1/2} \right)^\top \mathcal{P}(\bar{\mathbf{h}}_{i+\frac{1}{2}}) \bar{\mathbf{u}}_{i+\frac{1}{2}} + \frac{g}{2} \llbracket \mathbf{u} \rrbracket_{i+\frac{1}{2}}^\top \left(\overline{\mathcal{P}(\mathbf{h}) \mathbf{h}} \right)_{i+\frac{1}{2}} \\
&\stackrel{(4.8a)}{=} \frac{g}{2} \llbracket \mathcal{P}(\mathbf{h}) \mathbf{h} \rrbracket_{i+\frac{1}{2}}^\top \bar{\mathbf{u}}_{i+\frac{1}{2}} + g \llbracket \mathbf{B} \rrbracket_{i+\frac{1}{2}}^\top \mathcal{P}(\bar{\mathbf{h}}_{i+\frac{1}{2}}) \bar{\mathbf{u}}_{i+\frac{1}{2}} + \frac{g}{2} \llbracket \mathbf{u} \rrbracket_{i+\frac{1}{2}}^\top \left(\overline{\mathcal{P}(\mathbf{h}) \mathbf{h}} \right)_{i+\frac{1}{2}} \\
&\stackrel{(4.8b)}{=} \frac{g}{2} \llbracket \mathbf{u}^\top \mathcal{P}(\mathbf{h}) \mathbf{h} \rrbracket_{i+\frac{1}{2}} + g \llbracket \mathbf{B} \rrbracket_{i+\frac{1}{2}}^\top \mathcal{P}(\bar{\mathbf{h}}_{i+\frac{1}{2}}) \bar{\mathbf{u}}_{i+\frac{1}{2}} \\
&= \llbracket \Psi \rrbracket_{i+\frac{1}{2}} + g \llbracket \mathbf{B} \rrbracket_{i+\frac{1}{2}}^\top \mathcal{P}(\bar{\mathbf{h}}_{i+\frac{1}{2}}) \bar{\mathbf{u}}_{i+\frac{1}{2}},
\end{aligned}$$

which verifies (4.17), and hence lemma 4.4 is applicable, showing that this is an EC scheme. \square

4.3. A first-order ES scheme. The scheme determined by (4.12) numerically preserves the energy of the PDE system (1.1). However, it may lead to spurious oscillations since the energy should dissipate in the presence of shocks. The issue can be resolved by introducing appropriate numerical viscosity [27, 28, 14, 15, 16]. Our numerical diffusion operators are a straightforward stochastic extension of the energy-stable diffusion operators proposed in [14, 15].

For context of the approach, the introduction of a traditional Roe-type diffusion for a conservation law involves augmenting an EC flux as follows:

$$\mathcal{F}_{i+1/2}^{\text{RD}} := \mathcal{F}_{i+1/2}^{\text{EC}} - \frac{1}{2} \mathbf{Q}_{i+1/2}^{\text{Roe}} \llbracket \mathbf{U} \rrbracket_{i+1/2},$$

where \mathbf{Q}^{Roe} is a positive semi-definite matrix defined through a diagonalization of the interfacial flux Jacobian at a Roe-averaged state:

$$(4.20) \quad \mathbf{Q}_{i+\frac{1}{2}}^{\text{Roe}} := \mathbf{T}^{\text{Roe}} | \mathbf{\Lambda}^{\text{Roe}} | \left(\mathbf{T}^{\text{Roe}} \right)^{-1}, \quad \frac{\partial \hat{F}}{\partial \hat{U}} (\bar{\mathbf{U}}_{i+1/2}) = \mathbf{T}^{\text{Roe}} \mathbf{\Lambda}^{\text{Roe}} \left(\mathbf{T}^{\text{Roe}} \right)^{-1}.$$

Then the semi-discrete scheme (4.3) using the numerical flux $\mathcal{F}_{i+1/2} = \mathcal{F}_{i+1/2}^{\text{RD}}$ would behave like,

$$\begin{aligned} \frac{d}{dt} \mathbf{U}_i(t) &= -\frac{1}{\Delta x} \left(\mathcal{F}_{i+1/2}^{\text{EC}} - \mathcal{F}_{i-1/2}^{\text{EC}} \right) + \frac{1}{2\Delta x} \left(\mathbf{Q}_{i+1/2}^{\text{Roe}} \llbracket \mathbf{U} \rrbracket_{i+1/2} - \mathbf{Q}_{i-1/2}^{\text{Roe}} \llbracket \mathbf{U} \rrbracket_{i-1/2} \right) + \mathbf{S}_i \\ &\approx -\frac{1}{\Delta x} \left(\widehat{F}(\widehat{U})|_{x=x_{i+1/2}} - \widehat{F}(\widehat{U})|_{x=x_{i-1/2}} \right) + \Delta x \mathbf{Q} \widehat{U}_{xx}|_{x=x_i} + S(\widehat{U})|_{x=x_i}, \end{aligned}$$

where \mathbf{Q} is a positive-definite matrix, and hence this introduces diffusion into an EC scheme. While the above approach works in terms of adding a diffusion-like term, a convenient way to ensure energy stability is to employ a numerical diffusion term that operates on the entropic variables \mathbf{V} instead of the conservative variables \mathbf{U} :

$$(4.21) \quad \mathcal{F}_{i+\frac{1}{2}}^{\text{ES}} := \mathcal{F}_{i+\frac{1}{2}}^{\text{EC}} - \frac{1}{2} \mathbf{Q}_{i+\frac{1}{2}}^{\text{ES}} \llbracket \mathbf{V} \rrbracket_{i+\frac{1}{2}},$$

where $\mathbf{Q}_{i+\frac{1}{2}}^{\text{ES}}$ is a positive definite matrix that will be identified in a Roe-type way from the two adjacent states \mathbf{U}_i and \mathbf{U}_{i+1} at the cell interface $x = x_{i+\frac{1}{2}}$. The term \mathbf{V}_i is as given in (4.5b), and is a second-order approximation to the cell-average of the entropy variable \widehat{V} . We are interested in the Roe-type energy-stable operator defined as,

$$(4.22) \quad \mathcal{Q}_{i+1/2}(\mathbf{U}_i, \mathbf{U}_{i+1}) := \mathbf{T} |\mathbf{\Lambda}| \mathbf{T}^\top \geq 0,$$

where the matrices \mathbf{T} and $\mathbf{\Lambda}$ are matrices from the eigendecomposition of the flux Jacobian (2.14) evaluated at a Roe-type average state:

$$(4.23) \quad \frac{\partial \widehat{F}}{\partial \widehat{U}}(\tilde{\mathbf{U}}_{i+1/2}) = \mathbf{T} \mathbf{\Lambda} \mathbf{T}^{-1}, \quad \tilde{\mathbf{U}}_{i+1/2} := \begin{pmatrix} \bar{h}_{i+1/2} \\ \mathcal{P}(\bar{h}_{i+1/2}) \bar{\mathbf{u}}_{i+1/2} \end{pmatrix}.$$

Note in particular that $\bar{\mathbf{q}}_{i+1/2} \neq \mathcal{P}(\bar{h}_{i+1/2}) \bar{\mathbf{u}}_{i+1/2}$, so that $\tilde{\mathbf{U}}_{i+1/2} \neq \bar{\mathbf{U}}_{i+1/2}$. The focal scheme of this section uses the numerical flux (4.21), where \mathbf{Q} is given by the Roe-type diffusion matrix introduced above,

$$(4.24) \quad \mathbf{Q}_{i+\frac{1}{2}}^{\text{ES1}} := \mathcal{Q}_{i+1/2}(\mathbf{U}_i, \mathbf{U}_{i+1}) = \mathbf{T} |\mathbf{\Lambda}| \mathbf{T}^\top,$$

where we refer to this scheme as ‘‘ES1’’ because we will show it is first-order accurate. Our main result for this scheme is as follows.

Theorem 4.2 (ES1 scheme). *Consider the finite volume scheme (4.3) with source term (4.12b) and diffusive numerical flux (4.21), selecting the diffusion matrix as,*

$$(4.25) \quad \mathbf{Q}_{i+1/2}^{\text{ES}} = \mathbf{Q}_{i+1/2}^{\text{ES1}},$$

The resulting scheme is a first-order, well-balanced ES scheme.

Proof. We omit some details that are similar to the proof of theorem 4.1. We have already established in Theorem 4.1 that $\mathcal{F}_{i+1/2}^{\text{EC}}$ is second-order accurate. That this ES1 scheme is first-order is direct from the definition of \mathbf{V}_i in (4.5b), resulting in the approximation

$$\llbracket \mathbf{V} \rrbracket_{i+1/2} \approx \Delta x \widehat{V}_x(x_{i+1/2}).$$

which implies that the diffusive augmentation in (4.21) commits a first-order local truncation error.

To establish that this scheme is well-balanced, we assume the stochastic lake-at-rest initial data (4.13), and this coupled with the definition of \mathbf{V}_i in (4.5b) implies $\llbracket \mathbf{V} \rrbracket_{i+1/2} = 0$. Since the EC flux and source are well-balanced (lemma 4.2), then this implies that this ES1 scheme is also well-balanced.

Finally, we seek to show the ES property. We define the ES1 energy flux,

$$\mathcal{H}_{i+\frac{1}{2}}^{\text{ES1}} = \mathcal{H}_{i+\frac{1}{2}} - \frac{1}{2} \bar{\mathbf{V}}_{i+\frac{1}{2}}^\top \mathbf{Q}_{i+\frac{1}{2}}^{\text{ES1}} \llbracket \mathbf{V} \rrbracket_{i+\frac{1}{2}}.$$

with $\mathcal{H}_{i+1/2}$ as defined in (4.18). As in lemma 4.4, we multiply (4.3) by \mathbf{V}_i^\top ; after manipulations that are similar to those in the proof of lemma 4.4, we have,

$$\begin{aligned} \frac{d}{dt} \mathbf{E}_i(t) &= -\frac{1}{\Delta x} \left(\mathcal{H}_{i+\frac{1}{2}}^{ES1} - \mathcal{H}_{i-\frac{1}{2}}^{ES1} \right) \\ &\quad - \frac{1}{4\Delta x} \left(\llbracket \mathbf{V} \rrbracket_{i+\frac{1}{2}}^\top \mathbf{Q}_{i+\frac{1}{2}}^{ES1} \llbracket \mathbf{V} \rrbracket_{i+\frac{1}{2}} + \llbracket \mathbf{V} \rrbracket_{i-\frac{1}{2}}^\top \mathbf{Q}_{i-\frac{1}{2}}^{ES1} \llbracket \mathbf{V} \rrbracket_{i-\frac{1}{2}} \right). \end{aligned}$$

Since $\mathbf{Q}_{i+1/2}^{ES1}$ is positive semi-definite, then this scheme satisfies (4.11), and hence is an ES scheme. \square

4.4. ES1 diffusion vs Roe diffusion. We provide in this section a result that motivates and justifies our particular form of the ES1 diffusion modification defined in (4.24) and (4.25). This result states that if the bottom topography function vanishes (i.e., we are in the specialized case of a conservation law), then our chosen Roe-type ES1 diffusion in (4.22) and (4.23) coincides with a standard Roe-type diffusion term. Hence, in specialized scenarios our diffusive augmentations using entropic variables are equivalent to more standard Roe-type diffusion.

Proposition 4.1. *Define the Roe diffusion matrix as in (4.20), but using the flux Jacobian evaluated at $\tilde{\mathbf{U}}_{i+\frac{1}{2}}$,*

$$(4.26) \quad \frac{\partial \hat{\mathbf{F}}}{\partial \tilde{\mathbf{U}}}(\tilde{\mathbf{U}}_{i+\frac{1}{2}}) = \mathbf{T}^{Roe} \mathbf{\Lambda}^{Roe} (\mathbf{T}^{Roe})^{-1}.$$

where we have evaluated the flux jacobian at $\tilde{\mathbf{U}}_{i+1/2}$ instead of at $\bar{\mathbf{U}}_{i+1/2}$. Assume $\mathbf{B}_i = 0$ for all $i \in [M]$. Then,

$$(4.27) \quad \mathbf{Q}_{i+\frac{1}{2}}^{Roe} \llbracket \mathbf{U} \rrbracket_{i+\frac{1}{2}} = \mathbf{Q}_{i+\frac{1}{2}}^{ES1} \llbracket \mathbf{V} \rrbracket_{i+\frac{1}{2}}.$$

Proving this result requires some setup: Under the assumptions of proposition 4.1 we consider the SGSWE (2.12) with flat bottom, i.e., $\hat{B} = 0$, together with entropy $E^{\text{flat}}(\hat{\mathbf{U}}) = \frac{1}{2}(\hat{q})^\top \hat{u} + \frac{g}{2}\|\hat{h}\|^2$ and the entropy variables,

$$(4.28) \quad \hat{\mathbf{V}}^{\text{flat}} = \partial_{\hat{\mathbf{U}}} E = \begin{pmatrix} -\frac{1}{2}\mathcal{P}(\hat{u})\hat{u} + g\hat{h} \\ \hat{u} \end{pmatrix}.$$

Our main tool will be some results of the proof of Theorem 3.1 in [9]; in particular, while we have provided the flux Jacobian for this system in (2.14), we will need the explicit similarity transform that accomplishes its symmetrization.

Lemma 4.5 ([9], Theorem 3.1). *Assume $\mathcal{P}(\hat{h}) > 0$. Define $G = \sqrt{g\mathcal{P}(\hat{h})}$ as the positive definite square root matrix of $g\mathcal{P}(\hat{h})$. Then,*

$$\frac{\partial \hat{\mathbf{F}}}{\partial \hat{\mathbf{U}}}(\hat{\mathbf{U}}) = \mathbf{R} \mathbf{D} \mathbf{R}^{-1},$$

where \mathbf{D} is the symmetric matrix,

$$(4.29) \quad \mathbf{D}(\hat{\mathbf{U}}) = \frac{1}{2} \begin{pmatrix} 2G + \mathcal{P}(\hat{u}) + gG^{-1}\mathcal{P}(\hat{q})G^{-1} & \mathcal{P}(\hat{u}) - gG^{-1}\mathcal{P}(\hat{q})G^{-1} \\ \mathcal{P}(\hat{u}) - gG^{-1}\mathcal{P}(\hat{q})G^{-1} & \mathcal{P}(\hat{u}) + gG^{-1}\mathcal{P}(\hat{q})G^{-1} - 2G \end{pmatrix},$$

and

$$(4.30) \quad \mathbf{R}(\hat{\mathbf{U}}) = \frac{1}{\sqrt{2g}} \begin{pmatrix} I & I \\ \mathcal{P}(\hat{u}) + \sqrt{g\mathcal{P}(\hat{h})} & \mathcal{P}(\hat{u}) - \sqrt{g\mathcal{P}(\hat{h})} \end{pmatrix}.$$

The second lemma reveals the relation between the cell interface jump of \mathbf{V}^{flat} (the spatial approximation corresponding to the cell-averaged entropy variable $\hat{\mathbf{V}}^{\text{flat}}$ in (4.28)) and \mathbf{U} .

Lemma 4.6. Recall the definition of $\tilde{\mathbf{U}}_{i+\frac{1}{2}}$ in (4.23):

$$\tilde{\mathbf{U}}_{i+\frac{1}{2}} = \begin{pmatrix} \bar{\mathbf{h}}_{i+\frac{1}{2}} \\ \mathcal{P}(\bar{\mathbf{h}}_{i+\frac{1}{2}})\bar{\mathbf{u}}_{i+\frac{1}{2}} \end{pmatrix}$$

which is an intermediate state defined by the arithmetic average of \mathbf{h} and \mathbf{u} across the cell interface $x = x_{i+\frac{1}{2}}$. Denote, \mathbf{V}^{flat} to be the corresponding spatial approximation of the cell-averaged entropy variable defined in (4.28). Then,

(1) The jump $[[\mathbf{U}]]_{i+\frac{1}{2}}$ is a rescaling of the jump $[[\mathbf{V}^{flat}]]_{i+\frac{1}{2}}$, i.e.,

$$(4.31) \quad [[\mathbf{U}]]_{i+\frac{1}{2}} = (\mathbf{V}_{\mathbf{U}}^{flat})_{i+\frac{1}{2}} [[\mathbf{V}^{flat}]]_{i+\frac{1}{2}},$$

where

$$(\mathbf{V}_{\mathbf{U}}^{flat})_{i+\frac{1}{2}} := \frac{1}{g} \begin{pmatrix} I & \mathcal{P}(\bar{\mathbf{u}}_{i+\frac{1}{2}}) \\ \mathcal{P}(\bar{\mathbf{u}}_{i+\frac{1}{2}}) & \mathcal{P}^2(\bar{\mathbf{u}}_{i+\frac{1}{2}}) + g\mathcal{P}(\bar{\mathbf{h}}_{i+\frac{1}{2}}) \end{pmatrix},$$

$$[[\mathbf{V}^{flat}]]_{i+\frac{1}{2}} \stackrel{(4.28)}{=} \begin{pmatrix} -\frac{1}{2} [[\mathcal{P}(\mathbf{u})\mathbf{u}]]_{i+\frac{1}{2}} + g [[\mathbf{h}]]_{i+\frac{1}{2}} \\ [[\mathbf{u}]]_{i+\frac{1}{2}} \end{pmatrix}$$

(2) Let $\mathbf{R}_{i+\frac{1}{2}}$ denote the matrix that symmetrizes the flux Jacobian at the state $\tilde{\mathbf{U}}_{i+\frac{1}{2}}$,

$$\mathbf{R}_{i+\frac{1}{2}} := \mathbf{R}(\tilde{\mathbf{U}}_{i+\frac{1}{2}}) = \frac{1}{\sqrt{2g}} \begin{pmatrix} I & I \\ \mathcal{P}(\bar{\mathbf{u}}_{i+\frac{1}{2}}) + \sqrt{g\mathcal{P}(\bar{\mathbf{h}}_{i+\frac{1}{2}})} & \mathcal{P}(\bar{\mathbf{u}}_{i+\frac{1}{2}}) - \sqrt{g\mathcal{P}(\bar{\mathbf{h}}_{i+\frac{1}{2}})} \end{pmatrix},$$

cf. (4.30). Then,

$$(4.32) \quad \mathbf{R}_{i+\frac{1}{2}} \mathbf{R}_{i+\frac{1}{2}}^\top = (\mathbf{V}_{\mathbf{U}}^{flat})_{i+\frac{1}{2}}.$$

Proof. Part (2), i.e., (4.32), is a straightforward matrix algebra calculation that we omit. For part (1), we first recall that (4.8a) implies,

$$(4.33) \quad \frac{1}{2} [[\mathcal{P}(\mathbf{u})\mathbf{u}]]_{i+\frac{1}{2}} = \mathcal{P}(\bar{\mathbf{u}}_{i+\frac{1}{2}}) [[\mathbf{u}]]_{i+\frac{1}{2}}.$$

Second, we use the linearity of $\mathcal{P}(\cdot)$, the property (4.6) for arithmetic averages, and the commutation property (2.9), to conclude,

$$(4.34) \quad \mathcal{P}(\bar{\mathbf{u}}_{i+\frac{1}{2}}) [[\mathbf{h}]]_{i+\frac{1}{2}} + \mathcal{P}(\bar{\mathbf{h}}_{i+\frac{1}{2}}) [[\mathbf{u}]]_{i+\frac{1}{2}} = [[\mathcal{P}(\mathbf{h})\mathbf{u}]]_{i+\frac{1}{2}} = [[\mathbf{q}]]_{i+\frac{1}{2}}.$$

Therefore,

$$(\mathbf{V}_{\mathbf{U}}^{flat})_{i+\frac{1}{2}} [[\mathbf{V}^{flat}]]_{i+\frac{1}{2}} = \frac{1}{g} \begin{pmatrix} -\frac{1}{2} [[\mathcal{P}(\mathbf{u})\mathbf{u}]]_{i+\frac{1}{2}} + g [[\mathbf{h}]]_{i+\frac{1}{2}} + \mathcal{P}(\bar{\mathbf{u}}_{i+\frac{1}{2}}) [[\mathbf{u}]]_{i+\frac{1}{2}} \\ -\frac{1}{2} \mathcal{P}(\bar{\mathbf{u}}_{i+\frac{1}{2}}) [[\mathcal{P}(\mathbf{u})\mathbf{u}]]_{i+\frac{1}{2}} + g\mathcal{P}(\bar{\mathbf{u}}_{i+\frac{1}{2}}) [[\mathbf{h}]]_{i+\frac{1}{2}} + (\mathcal{P}^2(\bar{\mathbf{u}}_{i+\frac{1}{2}}) + g\mathcal{P}(\bar{\mathbf{h}}_{i+\frac{1}{2}})) [[\mathbf{u}]]_{i+\frac{1}{2}} \end{pmatrix}$$

$$\stackrel{(4.33)(4.34)}{=} \begin{pmatrix} [[\mathbf{h}]]_{i+\frac{1}{2}} \\ [[\mathbf{q}]]_{i+\frac{1}{2}} \end{pmatrix} = [[\mathbf{U}]]_{i+\frac{1}{2}}.$$

□

Now we are in position to show (4.27) in proposition 4.1.

Proof of proposition 4.1. Let $\mathbf{D}_{i+\frac{1}{2}}$ be the symmetric matrix defined in (4.29) evaluated at $\mathbf{U}_{i+\frac{1}{2}}$, and $\mathbf{D}_{i+\frac{1}{2}} = \mathbf{L}_{i+\frac{1}{2}} \mathbf{\Lambda}_{i+\frac{1}{2}} \mathbf{L}_{i+\frac{1}{2}}^\top$ be its eigenvalue decomposition. Then,

$$(4.35a) \quad \frac{\partial \widehat{F}}{\partial \widehat{\mathbf{U}}}(\tilde{\mathbf{U}}_{i+\frac{1}{2}}) = \mathbf{R}_{i+\frac{1}{2}} \left(\mathbf{L}_{i+\frac{1}{2}} \mathbf{\Lambda}_{i+\frac{1}{2}} \mathbf{L}_{i+\frac{1}{2}}^\top \right) \mathbf{R}_{i+\frac{1}{2}}^{-1}$$

$$(4.35b) \quad =: \mathbf{T}_{i+\frac{1}{2}} \mathbf{\Lambda}_{i+\frac{1}{2}} \mathbf{T}_{i+\frac{1}{2}}^{-1},$$

is an eigendecomposition of the Jacobian matrix $\frac{\partial \widehat{F}}{\partial \widetilde{U}}(\widetilde{U}_{i+\frac{1}{2}})$, where we have used the fact that $\mathbf{L}_{i+\frac{1}{2}}^{-1} = \mathbf{L}_{i+\frac{1}{2}}^\top$ due to the symmetry of $\mathbf{D}_{i+\frac{1}{2}}$. The Roe-diffusion operator evaluated at the location $\widetilde{U}_{i+\frac{1}{2}}$ as indicated in (4.26) is then given by,

$$\mathbf{Q}_{i+\frac{1}{2}}^{Roe} \stackrel{(4.20)}{=} \mathbf{T}_{i+\frac{1}{2}} |\boldsymbol{\Lambda}_{i+\frac{1}{2}}| \mathbf{T}_{i+\frac{1}{2}}^{-1}$$

Therefore,

$$\begin{aligned} \mathbf{Q}_{i+\frac{1}{2}}^{Roe} \llbracket \mathbf{U} \rrbracket_{i+\frac{1}{2}} &= \mathbf{T}_{i+\frac{1}{2}} |\boldsymbol{\Lambda}_{i+\frac{1}{2}}| \mathbf{T}_{i+\frac{1}{2}}^{-1} \llbracket \mathbf{U} \rrbracket_{i+\frac{1}{2}}, \\ &\stackrel{(4.35),(4.31)}{=} \left(\mathbf{R}_{i+\frac{1}{2}} \mathbf{L}_{i+\frac{1}{2}} \right) |\boldsymbol{\Lambda}_{i+\frac{1}{2}}| \left(\mathbf{R}_{i+\frac{1}{2}} \mathbf{L}_{i+\frac{1}{2}} \right)^{-1} (\mathbf{V}_{\mathbf{U}}^{\text{flat}})_{i+\frac{1}{2}} \llbracket \mathbf{V}^{\text{flat}} \rrbracket_{i+\frac{1}{2}}, \\ &\stackrel{(4.32)}{=} \left(\mathbf{R}_{i+\frac{1}{2}} \mathbf{L}_{i+\frac{1}{2}} \right) |\boldsymbol{\Lambda}_{i+\frac{1}{2}}| \left(\mathbf{R}_{i+\frac{1}{2}} \mathbf{L}_{i+\frac{1}{2}} \right)^{-1} \mathbf{R}_{i+\frac{1}{2}} \mathbf{R}_{i+\frac{1}{2}}^\top \llbracket \mathbf{V}^{\text{flat}} \rrbracket_{i+\frac{1}{2}}, \\ (4.36) \quad &= \mathbf{R}_{i+\frac{1}{2}} \left(\mathbf{L}_{i+\frac{1}{2}} |\boldsymbol{\Lambda}_{i+\frac{1}{2}}| \mathbf{L}_{i+\frac{1}{2}}^\top \right) \mathbf{R}_{i+\frac{1}{2}}^\top \llbracket \mathbf{V}^{\text{flat}} \rrbracket_{i+\frac{1}{2}}, \\ &= \mathbf{T}_{i+\frac{1}{2}} |\boldsymbol{\Lambda}_{i+\frac{1}{2}}| \mathbf{T}_{i+\frac{1}{2}}^\top \llbracket \mathbf{V}^{\text{flat}} \rrbracket_{i+\frac{1}{2}} \\ &\stackrel{(4.24)}{=} \mathbf{Q}_{i+\frac{1}{2}}^{ES1} \llbracket \mathbf{V}^{\text{flat}} \rrbracket_{i+\frac{1}{2}}. \end{aligned}$$

□

4.5. A second-order ES scheme. To develop a second-order accurate energy-stable scheme, we use jump operators with $O(\Delta x^2)$ accuracy. A natural choice is to use the jumps obtained by non-oscillatory second-order reconstructions of the entropy variable. However, attaining a provable energy-stable scheme requires the more subtle reconstruction procedure in [16] that we follow. The new idea for second-order diffusions is to use reconstructions in order to compute jumps. To that end, we let \mathbf{V}_i^+ and \mathbf{V}_{i+1}^- be second-order reconstructions from the right and left, respectively, of the entropy variable $\mathbf{V}(x)$ at location $x = x_{i+1/2}$. We will describe later in this section how these reconstructions are computed.

Assuming we have these reconstructions in hand, we can compute second-order accurate jumps of the entropy variables:

$$(4.37) \quad \langle\langle \mathbf{V} \rangle\rangle_{i+\frac{1}{2}} = \mathbf{V}_{i+1}^- - \mathbf{V}_i^+,$$

The overall scheme is similar as the previous section, but uses a second-order diffusive augmentation of a conservative flux,

$$(4.38) \quad \mathcal{F}_{i+\frac{1}{2}}^{ES2} := \mathcal{F}_{i+\frac{1}{2}}^{EC} - \frac{1}{2} \mathbf{Q}_{i+\frac{1}{2}}^{ES2} \langle\langle \mathbf{V} \rangle\rangle_{i+\frac{1}{2}}.$$

We choose the matrix \mathbf{Q}^{ES2} as for the ES1 scheme,

$$(4.39) \quad \mathbf{Q}_{i+1/2}^{ES2} = \mathbf{Q}_{i+1/2}^{ES1} = \mathcal{Q}_{i+1/2}(\mathbf{U}_i, \mathbf{U}_{i+1}) = \mathbf{T}_{i+1/2} |\boldsymbol{\Lambda}_{i+1/2}| \mathbf{T}_{i+1/2}^\top,$$

where we recall that the eigendecomposition matrices \mathbf{T} , $\boldsymbol{\Lambda}$ are computed from the Roe-type average of the flux Jacobian, cf. (4.22), (4.23). One could alternatively select \mathbf{Q}^{ES2} by using second-order reconstructions of \mathbf{U} as input to \mathcal{Q} , e.g.,

$$\mathbf{Q}_{i+1/2}^{ES2} = \mathcal{Q}_{i+1/2}(\mathbf{U}_i^-, \mathbf{U}_i^+),$$

for some second-order reconstructions \mathbf{U}_i^\pm .

What remain is to describe how \mathbf{V}_i^\pm are computed in a way that ensures the energy stable property. The main idea is to design \mathbf{V}_i^\pm through a second-order reconstruction of *scaled* (transformed) versions of the entropy variables:

$$(4.40) \quad \mathbf{w}_i^\pm := \mathbf{T}_{i\pm 1/2}^\top \mathbf{V}_i,$$

where the matrices $\mathbf{T}_{i\pm 1/2}$ are as in (4.39). Once these have been computed, we perform a second-order total variation-diminishing (TVD) reconstruction on the \mathbf{w} variable at the interfaces:

$$(4.41) \quad \tilde{\mathbf{w}}_i^\pm := \mathbf{w}_i^\pm \pm \frac{1}{2} \phi(\boldsymbol{\theta}_i^\pm) \circ \langle\langle \mathbf{w} \rangle\rangle_{i\pm 1/2},$$

where \circ is the Hadamard (elementwise) product on vectors, and $\boldsymbol{\theta}_i^\pm$ are difference quotients,

$$\boldsymbol{\theta}_i^\pm := \langle\langle \mathbf{w} \rangle\rangle_{i\mp 1/2} \oslash \langle\langle \mathbf{w} \rangle\rangle_{i\pm 1/2},$$

where \oslash is the Hadamard (elementwise) division between vectors. We select the function ϕ to be the minmod limiter,

$$(4.42) \quad \phi(\theta) = \begin{cases} 0, & \text{if } \theta < 0, \\ \theta, & \text{if } 0 \leq \theta \leq 1, \\ 1, & \text{otherwise.} \end{cases}$$

which operates elementwise on vector inputs. Note that other slope limiter functions ϕ may be selected, but minmod is the only valid limiter in this context that also satisfies the TVD property [16, Section 3.4]. Finally, the desired reconstructions for \mathbf{V}_i^\pm are defined by inverting the \mathbf{w} -to- \mathbf{V} map,

$$(4.43) \quad \mathbf{T}_{i\pm 1/2}^\top \mathbf{V}_i^\pm := \tilde{\mathbf{w}}_i^\pm$$

The full scheme has now been described, and satisfies the following properties.

Theorem 4.3 (ES2 scheme). *The FV scheme (4.3) choosing the flux $\mathcal{F}_{i+1/2} = \mathcal{F}_{i+1/2}^{ES2}$ defined in (4.38) is a second-order, well-balanced, ES scheme.*

We focus the remaining discussion in this section on sketching the proof of the above result. The second-order property results from the fact that the jumps are computed using second-order accurate reconstructions; the well-balanced property can be proven in exactly the same way as is done for the ES1 scheme in the proof of theorem 4.2. To show the ES property, we exercise one of the major results in [16] that we reproduce below.

Lemma 4.7 ([16], Lemma 3.2). *For each i , if there exists a positive diagonal matrix $\mathbf{\Pi}_{i+1/2} \geq 0$ such that the second-order jump satisfies,*

$$(4.44) \quad \langle\langle \mathbf{V} \rangle\rangle_{i+\frac{1}{2}} = (\mathbf{T}_{i+\frac{1}{2}}^\top)^{-1} \mathbf{\Pi}_{i+\frac{1}{2}} \mathbf{T}_{i+\frac{1}{2}}^\top \llbracket \mathbf{V} \rrbracket_{i+\frac{1}{2}},$$

then the scheme (4.3) with flux term $\mathcal{F}_{i+1/2} = \mathcal{F}_{i+1/2}^{ES2}$ is an ES scheme.

Hence, showing the ES property for our scheme only requires us to establish (4.44). To accomplish this, note that the definition (4.41) implies,

$$(4.45) \quad \langle\langle \tilde{\mathbf{w}} \rangle\rangle_{i+\frac{1}{2}}^\ell = \left(1 - \frac{1}{2} \phi((\boldsymbol{\theta}_{i+1}^-)^\ell) - \frac{1}{2} \phi((\boldsymbol{\theta}_i^+)^\ell) \right) \langle\langle \mathbf{w} \rangle\rangle_{i+\frac{1}{2}}^\ell,$$

I.e., we have,

$$(4.46) \quad \langle\langle \tilde{\mathbf{w}} \rangle\rangle_{i+\frac{1}{2}} = \mathbf{\Pi}_{i+\frac{1}{2}} \langle\langle \mathbf{w} \rangle\rangle_{i+\frac{1}{2}}, \quad (\mathbf{\Pi}_{i+1/2})_{\ell,\ell} := \left(1 - \frac{1}{2} \phi((\boldsymbol{\theta}_{i+1}^-)_\ell) - \frac{1}{2} \phi((\boldsymbol{\theta}_i^+)_\ell) \right)$$

and in particular $\mathbf{\Pi}_{i+1/2}$ is a diagonal matrix and positive semi-definite since $0 \leq \phi(\theta) \leq 1$. Since the jump operators $\langle\langle \cdot \rangle\rangle$ and $\llbracket \cdot \rrbracket$ are linear in their arguments, then combining (4.45) with the relations (4.40) and (4.43) that connect \mathbf{w}_i and $\tilde{\mathbf{w}}_i$ to \mathbf{V}_i and \mathbf{V}_i^\pm yields the relation (4.44) with a positive-definite diagonal matrix $\mathbf{\Pi}_{i+1/2}$. Hence, this is an ES scheme, and completes the proof of theorem 4.3.

Finally, we remark that the implementation of the diffusion term in the ES2 flux (4.38) does not require explicit construction of \mathbf{V}_i^\pm . I.e., we have,

$$\begin{aligned} \frac{1}{2} \mathbf{Q}_{i+\frac{1}{2}}^{ES2} \langle\langle \mathbf{V} \rangle\rangle_{i+\frac{1}{2}} &\stackrel{(4.22),(4.44)}{=} \frac{1}{2} \mathbf{T}_{i+\frac{1}{2}} |\mathbf{\Lambda}_{i+\frac{1}{2}}| \mathbf{T}_{i+\frac{1}{2}}^\top (\mathbf{T}_{i+\frac{1}{2}}^\top)^{-1} \mathbf{\Pi}_{i+\frac{1}{2}} \mathbf{T}_{i+\frac{1}{2}}^\top \llbracket \mathbf{V} \rrbracket_{i+\frac{1}{2}} \\ &= \frac{1}{2} \mathbf{T}_{i+\frac{1}{2}} |\mathbf{\Lambda}_{i+\frac{1}{2}}| \mathbf{\Pi}_{i+\frac{1}{2}} \mathbf{T}_{i+\frac{1}{2}}^\top \llbracket \mathbf{V} \rrbracket_{i+\frac{1}{2}} \\ &\stackrel{(4.40)}{=} \frac{1}{2} \mathbf{T}_{i+\frac{1}{2}} |\mathbf{\Lambda}_{i+\frac{1}{2}}| \mathbf{\Pi}_{i+\frac{1}{2}} \langle\langle \mathbf{w} \rangle\rangle_{i+\frac{1}{2}}, \\ &\stackrel{(4.46)}{=} \frac{1}{2} \mathbf{T}_{i+\frac{1}{2}} |\mathbf{\Lambda}_{i+\frac{1}{2}}| \langle\langle \tilde{\mathbf{w}} \rangle\rangle_{i+\frac{1}{2}}, \end{aligned}$$

and hence one need only compute $\tilde{\mathbf{w}}_i^\pm$ in order to directly evaluate the diffusion part of the ES2 flux.

4.6. Algorithmic details. Our overall scheme is the semi-discrete form (4.3), which we pair with a numerical time-stepping scheme. We provide pseudocode in this section that describes a fully discrete SGSWE time-stepping algorithm. This full pseudocode introduces some additional details for the scheme that were devised in [9], many of which are based on standard procedures used in schemes for deterministic SWE models [18]. We very briefly describe these additional details in the coming sections; more comprehensive discussion can be found in [9]. The full algorithmic pseudocode is given in algorithm 1.

4.6.1. Velocity desingularization. Computing \mathbf{u}_i requires inversion of the matrix $\mathcal{P}(\mathbf{h}_i)$, which is assumed (and enforced in the scheme) to be symmetric and positive-definite. However, this matrix may be ill-conditioned. To ameliorate numerical artifacts associated with this ill-conditioned operation, we employ a *desingularization* procedure, introduced for the deterministic SWE in [20]. We describe here the stochastic variant of the desingularization procedure, proposed in [9]. If $\mathcal{P}(\mathbf{h}_i)$ has the eigenvalue decomposition,

$$\mathcal{P}(\mathbf{h}_i) = \mathbf{Q} \mathbf{\Pi} \mathbf{Q}^\top, \quad \mathbf{\Pi} = \text{diag}(\pi_1, \dots, \pi_K),$$

where $\pi_k > 0$ are the eigenvalues of $\mathcal{P}(\mathbf{h}_i)$, then the desingularization process approximates $\mathcal{P}(\mathbf{h}_i)^{-1} \mathbf{q}_i$ by regularizing the matrix inverse procedure:

$$(4.47) \quad \mathbf{u}_i = \mathbf{Q} \tilde{\mathbf{\Pi}}^{-1} \mathbf{Q}^\top \mathbf{q}_i, \quad \mathbf{\Pi} = \text{diag}(\tilde{\pi}_1, \dots, \tilde{\pi}_K), \quad \tilde{\pi}_k = \frac{\sqrt{\pi_k^4 + \max\{\pi_k^4, \epsilon^4\}}}{\sqrt{2}\pi_k},$$

where $\epsilon > 0$ is a small constant; we choose it to be $\epsilon = \Delta x$. Note that if $\pi_k \geq \epsilon^{1/4}$, then $\tilde{\pi}_k = \pi_k$, and hence regularization is performed only in the presence of small eigenvalues. Compared to (4.4). This procedure to compute \mathbf{u}_i is a stabilized way to compute velocities.

For scheme consistency, if the desingularization above is activated, then we recompute the discharge variable:

$$\mathbf{q}_i \leftarrow \mathcal{P}(\mathbf{h}_i) \mathbf{u}_i.$$

4.6.2. Hyperbolicity preservation. The SGSWE PDE (2.12) is hyperbolic and has an entropy pair if $\mathcal{P}(\hat{h}) > 0$, i.e., Theorems 2.1 and 3.1, respectively. To ensure this holds at the discrete level, we require the condition $\mathcal{P}(\mathbf{h}_i) > 0$ for every cell i . To enforce this, we employ [9, Theorem 3.4, Corollary 3.5], which state that a sufficient condition for $\mathcal{P}(\mathbf{h}_i) > 0$ is that for every $m = 1, \dots, M$,

$$(4.48) \quad \hat{h}_i(\xi_m) > 0, \quad \hat{h}_i(\xi) := \sum_{k=1}^K \mathbf{h}_{i,k} \phi_k(\xi_m), \quad \mathbf{h}_i = (\mathbf{h}_{i,1}, \dots, \mathbf{h}_{i,K})^\top,$$

where $\{\xi_m\}_{m=1}^M$ is a nodal set in \mathbb{R}^d for a positive-weight quadrature rule having sufficient accuracy relative to the ξ -polynomial space P defined in (2.4). The functions ϕ_k are the basis of P in (2.4) for which \mathbf{h}_i are coordinates. The function $\hat{h}_i(\xi)$ is the SGSWE approximation to the \mathcal{I}_i -cell average of $\hat{h}(x, t, \xi)$ at the current time. Hence, the computational vehicle we use to enforce hyperbolicity

of the underlying PDE in our scheme is to enforce the above positivity-type condition on the \mathbf{h}_i variable.

4.6.3. Positivity-preservation. We enforce the positivity condition (4.48) by restricting the timestep size. We assume that the current time value of \mathbf{h}_i satisfies (4.48). If Forward Euler with a stepsize Δt is used to discretize (4.3), then (4.48) is true at the next time step if,

$$(4.49) \quad \Delta t < \lambda := \min_i \min_{m=1, \dots, M} \left| \frac{\Delta x \hat{h}_i(\xi_m)}{\hat{\mathcal{F}}_{i+1/2}^h(\xi_m) - \hat{\mathcal{F}}_{i-1/2}^h(\xi_m)} \right|,$$

where $\hat{\mathcal{F}}_{i+1/2}^h(\cdot)$ is the SG approximation of the \hat{h} -variable flux:

$$\hat{\mathcal{F}}_{i+1/2}^h(\xi) := \sum_{k=1}^K \mathcal{F}_{i+1/2,k}^h \phi_k(\xi), \quad \mathcal{F}_{i+1/2} = \left(\left(\mathcal{F}_{i+1/2}^h \right)^\top, \left(\mathcal{F}_{i+1/2}^q \right)^\top \right)^\top \in \mathbb{R}^{2K}.$$

Hence, we enforce positivity preservation by ensuring a small enough timestep so that the positivity condition (4.48) is respected globally over all spatial cells. We must also restrict Δt to satisfy the wave speed CFL condition; see [9, Equation (4.16)].

4.6.4. Adaptive time-stepping. The time step restriction (4.49) works for Forward Euler time-stepping. To extend this to a higher-order temporal scheme, we employ a third-order strong stability-preserving scheme, which is a convex combination of Forward Euler steps [17]. However, the intermediate stages of a(ny) time-stepping scheme need not obey the positivity-preserving property, even if Δt is chosen to obey the condition (4.49) determined at the initial step.

To address this issue, we employ the *adaptive* time-stepping strategy proposed in [5, Remark 3.6]. We refer the reader to that reference for details, and present here only a high-level description of the procedure: λ is initialized as the initial stage value of λ , as shown in (4.49). At intermediate stages, new intermediate values of λ are computed. If an intermediate-stage value of λ is smaller than the current value of λ , then we restart the entire time-step using the new, smaller- λ restriction on Δt .

5. NUMERICAL EXPERIMENTS

Below we present several numerical examples to illustrate properties of the developed schemes. We refer to the second order energy-conservative scheme, the first order energy-stable scheme, and the second order energy-stable scheme as the EC, ES1, and ES2 schemes, respectively. We introduce the relative change in energy quantity,

$$(5.1) \quad \text{relative energy} = \frac{E(t) - E(0)}{E(t)},$$

where $E(t)$ is computed as $\sum_i \Delta x \mathbf{E}_i(t)$. This provides a way to visualize the relative change in the discrete energy for different numerical schemes, namely for the EC, ES1 and ES2. In all tests below we consider a single (scalar) random variable ξ that is a uniformly distributed random variable on $[-1, 1]$; hence our choice for the functions ϕ_k are orthonormal Legendre polynomials on $[-1, 1]$. We use $K = 9$ for the dimension of the PC space P . Instead of visualizing the conservative variable h corresponding to water height, we will plot the *water surface* w , defined as $w = h + B$, with the bottom topography B superimposed on the same graph; plots of (w, B) are more physically interpretable than directly plotting the water height h .

5.1. Flat-Bottom Dam Break. In the first experiment, we consider a stochastic water surface,

$$h(x, 0, \xi) + B(x, 0, \xi) = w(x, 0, \xi) = \begin{cases} 2.0 + 0.1\xi & x < 0 \\ 1.5 + 0.1\xi & x > 0 \end{cases}, \quad q(x, 0, \xi) = 0,$$

with a flat bottom $B(x, t, \xi) \equiv 0$. This is a stochastic modification of the deterministic ‘‘dam break test’’ problem from [15]. In fig. 1, we use a uniform grid size $\Delta x = 400$ over the physical domain $x \in [-1, 1]$, and compute up to the time $t = 0.4$. We test the example using different numerical methods (EC, ES1, ES2), Section 4.

Algorithm 1 The fully discrete SGSWE schemes proposed in this paper; we ignore specifying the handling of boundary conditions.

Input scheme type: `scheme = EC, ES1, or ES2`

Input: Bottom topography B , initial data $U(t = 0)$, polynomial index set Λ

Input: Terminal time T

Initialize: $U_i, t = 0$

repeat

 Compute B_i from B for all i

 Compute u_i in (4.47) for all i

 Compute $\mathcal{F}_{i+1/2}^{EC}$ for all i , given by (4.12)

if `scheme` is `EC` **then** for all i :

 Set $\mathcal{F}_{i+1/2} \leftarrow \mathcal{F}_{i+1/2}^{EC}$.

else for all i :

 Compute entropy variable V_i using (4.5b).

 Compute $T_{i+1/2}, \Lambda_{i+1/2}$ through (4.23).

if `scheme` is `ES1` **then**:

 Compute $Q_{i+1/2}^{ES1}$ using (4.23),(4.24) with $T_{i+1/2}, \Lambda_{i+1/2}$.

 Compute $\mathcal{F}_{i+1/2} \leftarrow \mathcal{F}_{i+1/2}^{ES}$ in (4.21) using $\mathcal{F}_{i+1/2}^{EC}, V_i$, and $Q_{i+1/2}^{ES} \leftarrow Q_{i+1/2}^{ES1}$.

else if `scheme` is `ES2` **then**:

 Construct $Q_{i+1/2}^{ES2}$ as in (4.39) with $T_{i+1/2}, \Lambda_{i+1/2}$.

 Construct V_i^\pm through (4.40), (4.41), and (4.43).

 Compute $\mathcal{F}_{i+1/2} \leftarrow \mathcal{F}_{i+1/2}^{ES2}$ in (4.38) and (4.37) using $Q_{i+1/2}^{ES2}, V_i^\pm$, and $\mathcal{F}_{i+1/2}^{EC}$.

end if

end if

 Initialize λ and Δt as shown in (4.49).

 Adaptively determine Δt using the procedure discussed in section 4.6.4.

 Use a third-order SSP method to take a time step of size Δt , updating h_i and q_i .

 Set $t \leftarrow t + \Delta t$.

until $t \geq T$

From fig. 1, similar to the results presented in [15, Figs. 1 and 4], we observe that the water surface with uncertainties develops a leftward-going rarefaction wave and a rightward-going shock. Similar to [15], EC computes such solutions accurately, but at the expense of large post-shock oscillations as observed on fig. 1 (right plot). These oscillations are expected since the EC scheme preserves energy, and hence energy is not dissipated across the shock as it should. We also demonstrate on fig. 2 (middle and right plots) the numerical energy conservation for the EC scheme. We note that the energy conservation errors due to time discretization are reduced significantly by decreasing the time step/CFL constant (right figure), similar to the results reported in fig. 1 in [15]. The presented results in fig. 1 and fig. 2 (left figure) also illustrate that ES2 produces less smearing than the ES1 at both the rarefaction and the shock waves. The schemes ES1 and ES2 are both designed to dissipate energy which is also confirmed by the numerical experiments as presented in fig. 2 (middle plot), with the energy dissipation in the ES2 being lower than in the ES1 scheme. In addition, the numerical results seem to indicate that the ES2 scheme is better able to capture large variance spikes compared to the ES1 scheme. Finally, the employment of the numerical diffusion operators in ES1 and ES2 schemes, removes oscillations present in the numerical solution using the EC scheme. The observed results are also in agreement with the results of the deterministic model reported in [15].

5.2. Stochastic Bottom Topography. Next, we consider the shallow water system with deterministic initial conditions,

$$w(x, 0) = \begin{cases} 1 & x < 0 \\ 0.5 & x > 0 \end{cases}, \quad q(x, 0) = 0,$$

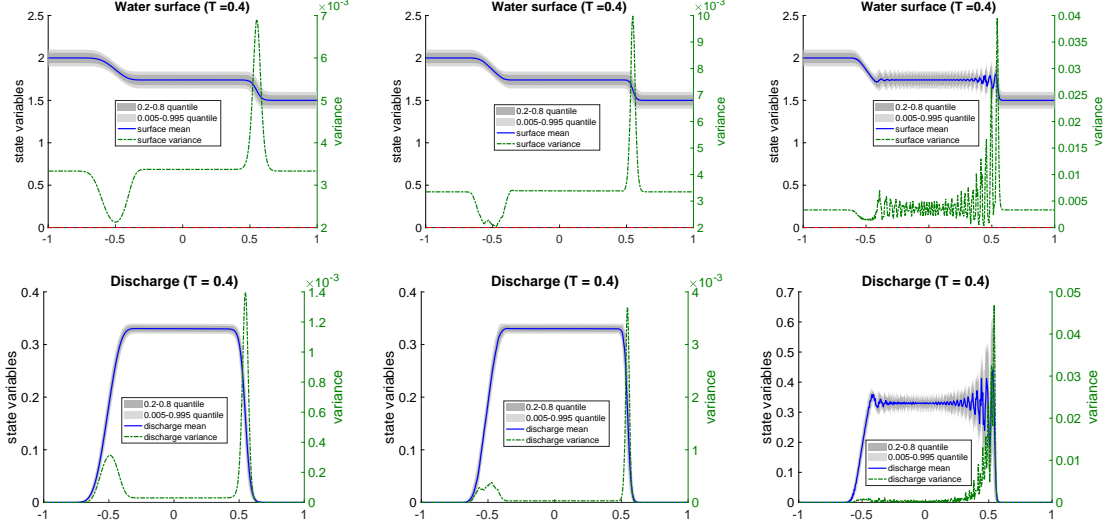


FIGURE 1. Results for section 5.1. Top: water surface, Bottom: discharge: Left: ES1. Middle: ES2. Right: EC. Mesh $n_x = 400$ and PC basis functions $K=9$.

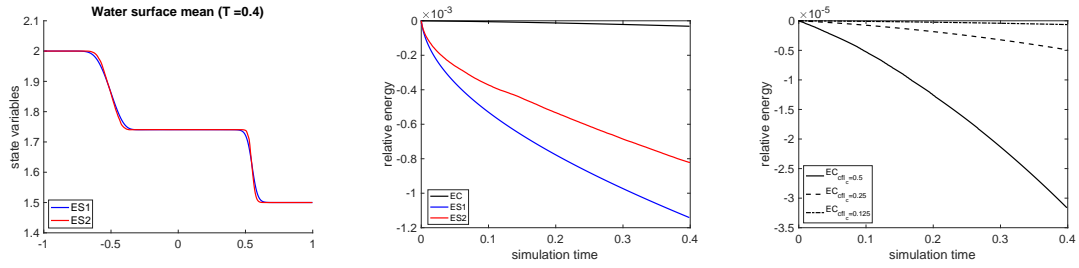


FIGURE 2. Results for section 5.1. Comparison: Left - water surface mean ES1 vs. ES2. Middle: relative energy change in EC, ES1, ES2. Right: relative energy change in EC under different time step/CFL constant. Mesh $n_x = 400$ and PC basis functions $K=9$.

and with a stochastic bottom topography,

$$(5.2) \quad B(x, \xi) = \begin{cases} 0.125(\cos(5\pi x) + 2) + 0.125\xi, & |x| < 0.2 \\ 0.125 + 0.125\xi, & \text{otherwise.} \end{cases}$$

This test example was presented previously in [9]. Initially, the highest possible bottom barely touches the initial water surface at $x = 0$, see fig. 3-fig. 5. In fig. 3-fig. 5, we use a uniform grid size $\Delta x = 400, 800, 1600$ over the physical domain $x \in [-1, 1]$, and compute up to time $t = 0.0995$ (Immediately after this time, the EC scheme fails for an $n_x=400$ due to spurious oscillations near sharp gradients of the solution). In fig. 4-fig. 5 we compare only performance of ES1 and ES2 at $t = 0.0995$ since EC fails on those meshes even earlier. Again, the numerical results indicate that the ES2 scheme can more easily resolve large, spatially-concentrated variance values compared to the ES1 scheme, but under mesh refinement both schemes converge to similar numerical solutions. In fig. 6, we show numerical solution obtained using ES1 and ES2 at the final time $t = 0.8$ and on mesh $n_x = 800$. For both schemes, the 99% confidence region of the water surface stays above the 99% confidence region of the bottom function in fig. 6, and both methods produce similar numerical solutions. The presented results are comparable to the results in [9, Section 5.1]. In fig. 7, we again

observe as expected that the EC scheme numerically conserves energy, while ES1 and ES2 dissipate energy with larger dissipation produced by ES1 method.

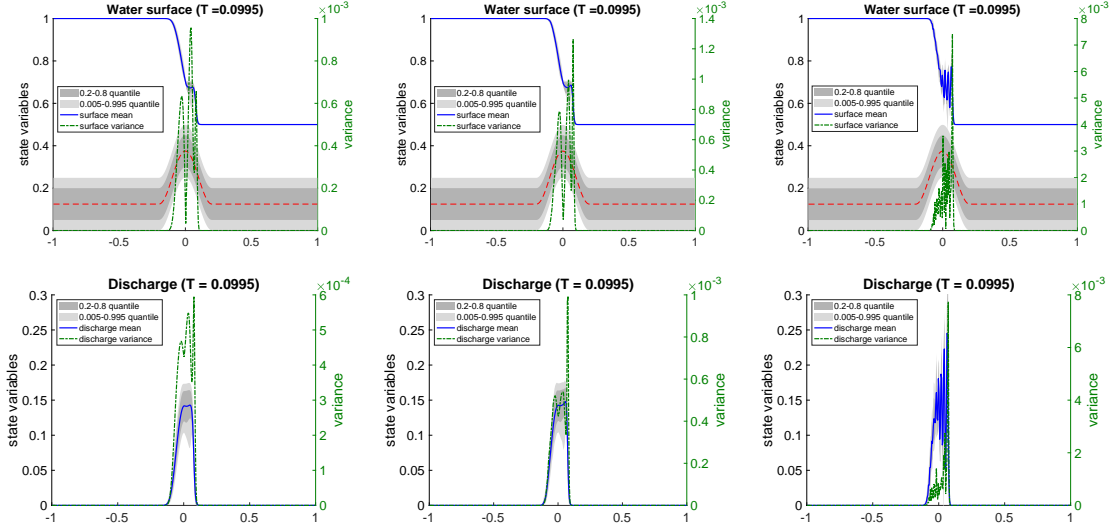


FIGURE 3. Comparison of the results for section 5.2 using different schemes. Top: water surface. Bottom: discharge. Left: ES1, Middle: ES2, Right: EC. Mesh $nx = 400$ with $K = 9$ at earlier time $T = 0.0995$.

5.3. Perturbation to Lake at Rest. As a final example, we consider the shallow water system with stochastic water surface,

$$(5.3) \quad w(x, 0, \xi) = \begin{cases} 1 + 0.001(\xi + 1) & |x| \leq 0.05 \\ 1 & \text{otherwise} \end{cases}, \quad q(x, 0, \xi) = 0,$$

and with a deterministic bottom topography

$$(5.4) \quad B(x) = \begin{cases} 0.25(\cos(5\pi(x + 0.35)) + 1), & -0.55 < x < -0.15 \\ 0.125(\cos(10\pi(x - 0.35)) + 1), & 0.25 < x < 0.45 \\ 0, & \text{otherwise.} \end{cases}$$

The test is from [6] and is similar to the deterministic tests of the perturbation of lake at rest solution, for example to the one presented in [15]. From presented results in fig. 8, fig. 9 and fig. 10, we make conclusions similar to previous sections: Both ES1 and ES2 capture small stochastic perturbations of the lake at rest solution quite well (with both leftward- and rightward- going waves present in the numerical solutions). The first order ES1 scheme exhibits much more dissipation in the left and the right going waves than the ES2 scheme, which produces a more accurate solution, as shown in fig. 8, fig. 9 (left and middle figures), fig. 10. The results of EC scheme is also shown in fig. 9 (right figure). The EC scheme resolves the left and the right going water waves with heights higher than in both ES1 and ES2 methods, but again there are oscillations present near both waves in EC numerical solution as expected since EC does not dissipates energy across shocks. The relative energy change for this example produced by EC, ES1 and ES2 methods is illustrated in fig. 11. The presented results are also comparable to the results reported in [15] and in [6].

6. CONCLUSION

In this work we derived an entropy-entropy flux pair for the spatially one-dimensional hyperbolicity-preserving, positivity-preserving SG SWE system developed in [9]. Such entropy-entropy flux

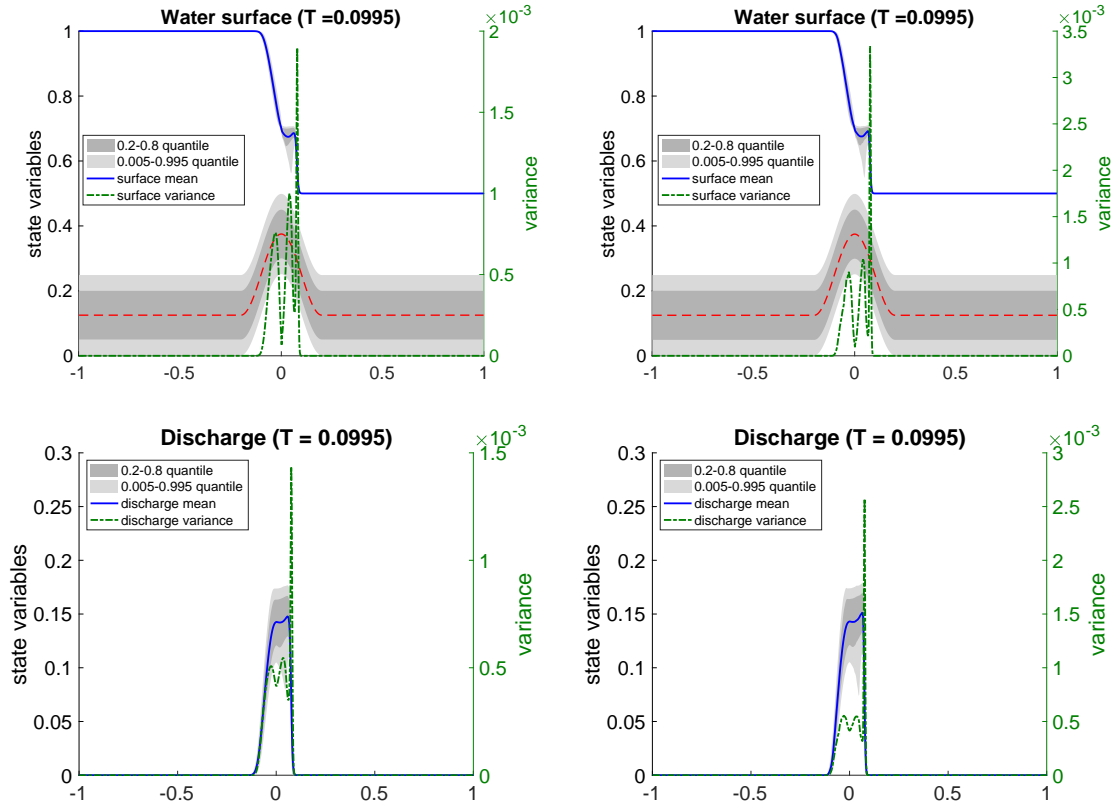


FIGURE 4. Comparison of the results for section 5.2 using different schemes. Top: water surface. Bottom: discharge. Left: ES1, Right: ES2. Mesh $nx = 800$ with $K = 9$ at earlier time $T = 0.0995$.

pairs are the theoretical starting point for proposing entropy admissibility criteria to resolve non-uniqueness of weak solutions. Next, using the proposed entropy-entropy flux pair, we designed second-order energy conservative, and first- and second-order energy stable finite volume schemes for the SG SWE. The proposed schemes are also well-balanced. We provided several numerical experiments to illustrate performance of the methods. As a part of future research, we plan to extend such methods to models in two spatial dimensions, to explore alternative constructions of the diffusion operators, and to investigate other reconstruction approaches for the entropy variables.

7. ACKNOWLEDGEMENT

The work of Yekaterina Epshteyn and Akil Narayan was partially supported by NSF DMS-2207207. AN was partially supported by NSF DMS-1848508.

REFERENCES

1. Adhémar-Jean-Claude Barré de Saint-Venant, *Théorie du mouvement non permanent des eaux, avec application aux crues des rivières et à l'introduction des marées dans leur lit*, (1871) (français).
2. Sylvie Benzoni-Gavage and Denis Serre, *Multi-dimensional hyperbolic partial differential equations: First-order systems and applications*, Oxford University Press on Demand, 2007.
3. Alfredo Bermudez and Ma Elena Vazquez, *Upwind methods for hyperbolic conservation laws with source terms*, *Computers & Fluids* **23** (1994), no. 8, 1049–1071.
4. Steve Bryson, Yekaterina Epshteyn, Alexander Kurganov, and Guergana Petrova, *Well-balanced positivity preserving central-upwind scheme on triangular grids for the Saint-Venant system*, *ESAIM: Mathematical Modelling and Numerical Analysis* **45** (2011), no. 3, 423–446.

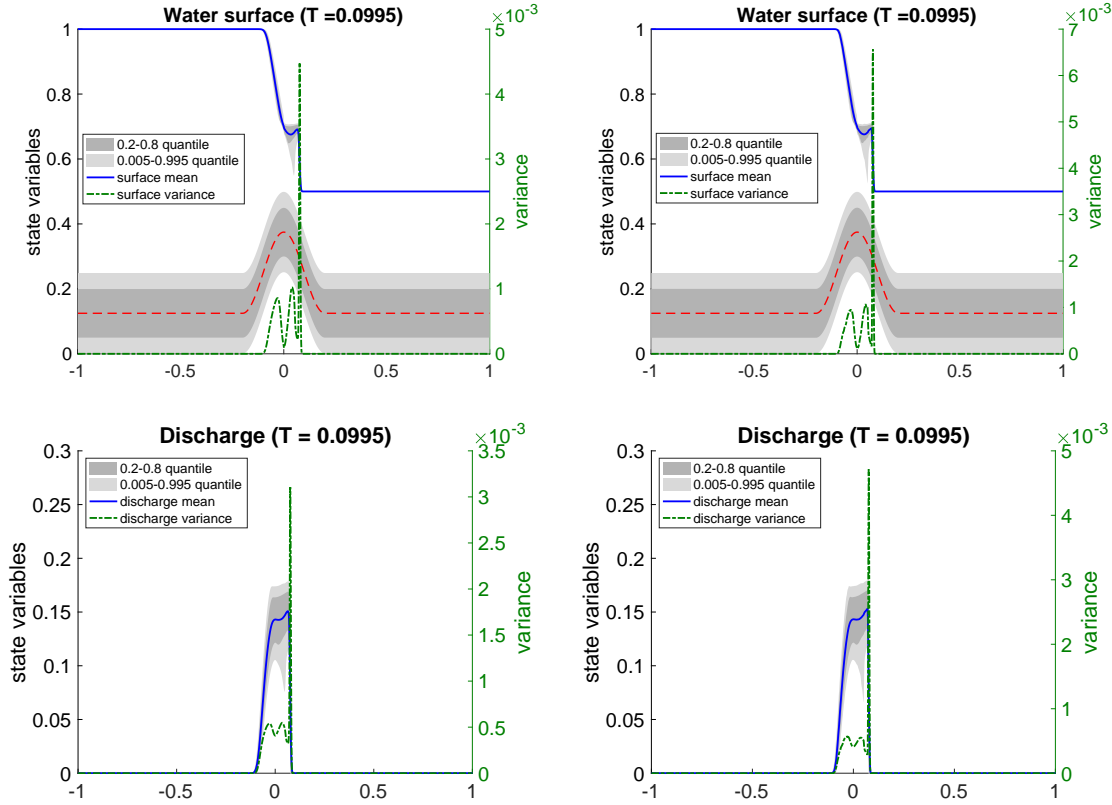


FIGURE 5. Comparison of the results for section 5.2 using different schemes. Top: water surface. Bottom: discharge. Left: ES1, Right: ES2. Mesh $n_x = 1600$ with $K = 9$ at earlier time $T = 0.0995$.

5. A. Chertock, S. Cui, A. Kurganov, and T. Wu, *Well-balanced positivity preserving central-upwind scheme for the shallow water system with friction terms*, International Journal for Numerical Methods in Fluids **78** (2015), no. 6, 355–383.
6. A. Chertock, S. Jin, and A. Kurganov, *A well-balanced operator splitting based stochastic Galerkin method for the one-dimensional Saint-Venant system with uncertainty*, (2015), preprint.
7. Albert Cohen and Ronald DeVore, *Approximation of high-dimensional parametric PDEs*, Acta Numerica **24** (2015), 1–159.
8. Constantine M Dafermos, *Hyperbolic conservation laws in continuum physics*, Springer, 2016.
9. Dihan Dai, Yekaterina Epshteyn, and Akil Narayan, *Hyperbolicity-Preserving and Well-Balanced Stochastic Galerkin Method for Shallow Water Equations*, SIAM Journal on Scientific Computing **43** (2021), no. 2, A929–A952.
10. ———, *Hyperbolicity-preserving and well-balanced stochastic Galerkin method for two-dimensional shallow water equations*, Journal of Computational Physics **452** (2022), 110901.
11. Bert J Deusschere, Habib N Najm, Philippe P Pébay, Omar M Knio, Roger G Ghanem, and Olivier P Le Maître, *Numerical Challenges in the Use of Polynomial Chaos Representations for Stochastic Processes*, SIAM journal on scientific computing **26** (2004), no. 2, 698–719.
12. Yekaterina Epshteyn and Thuong Nguyen, *Adaptive central-upwind scheme on triangular grids for the Saint-Venant system*, Communications in Mathematical Sciences **21** (2023), no. 3, 671–708.
13. Oliver G. Ernst, Antje Mugler, Hans-Jörg Starkloff, and Elisabeth Ullmann, *On the Convergence of Generalized Polynomial Chaos Expansions*, ESAIM: Mathematical Modelling and Numerical Analysis **46** (2012), no. 02, 317–339.
14. Ulrik Fjordholm, Siddhartha Mishra, and Eitan Tadmor, *Energy preserving and energy stable schemes for the shallow water equations*, London Mathematical Society Lecture Note Series, p. 93–139, Cambridge University Press, 2009.

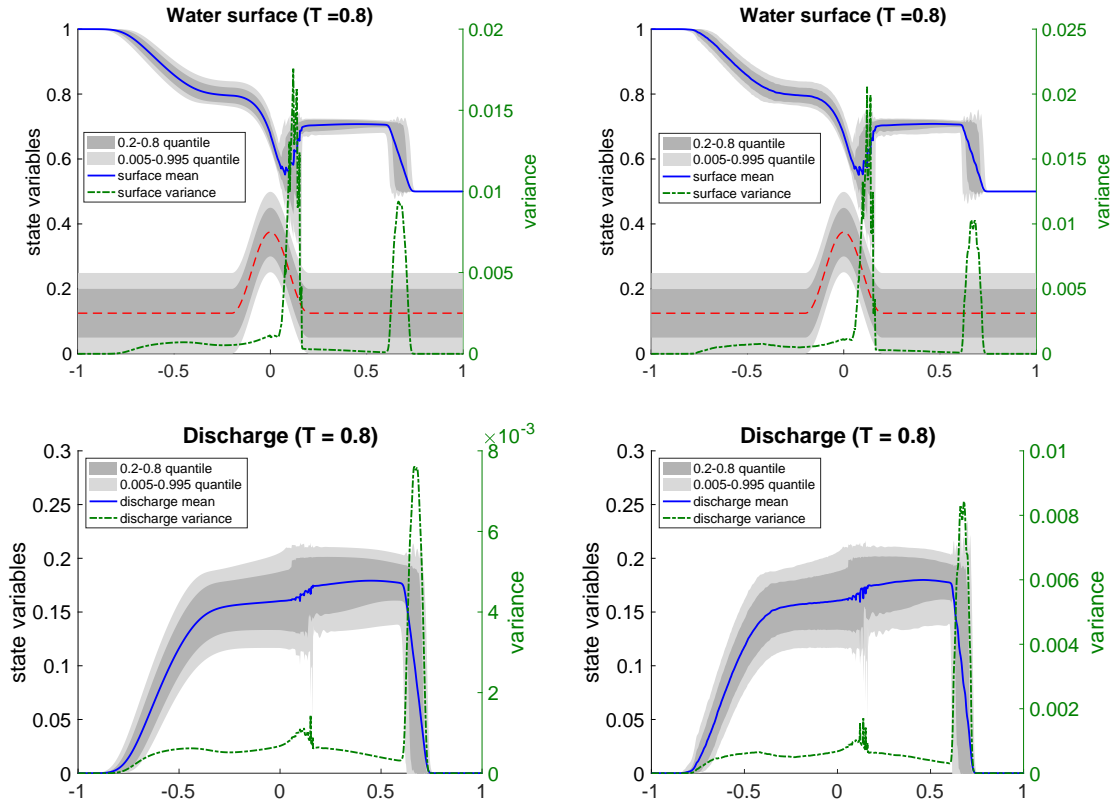


FIGURE 6. Comparison of the results for section 5.2 using different schemes. Top: water surface. Bottom: discharge. Left: ES1, and Right: ES2. Mesh $n_x = 800$ with $K = 9$ at the final time $T = 0.8$.

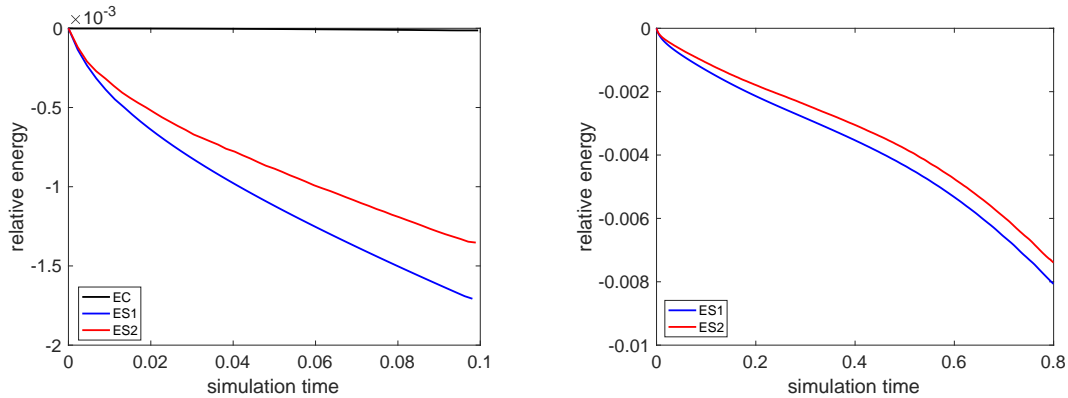


FIGURE 7. Comparison of the results for section 5.2 using different schemes. Relative energy change: Left: EC vs. ES1 vs. ES2 on mesh $n_x = 400$ on time interval $[0, 0.0995]$. Right: ES1 vs. ES2 on mesh $n_x = 800$ on time interval $[0, 0.8]$.

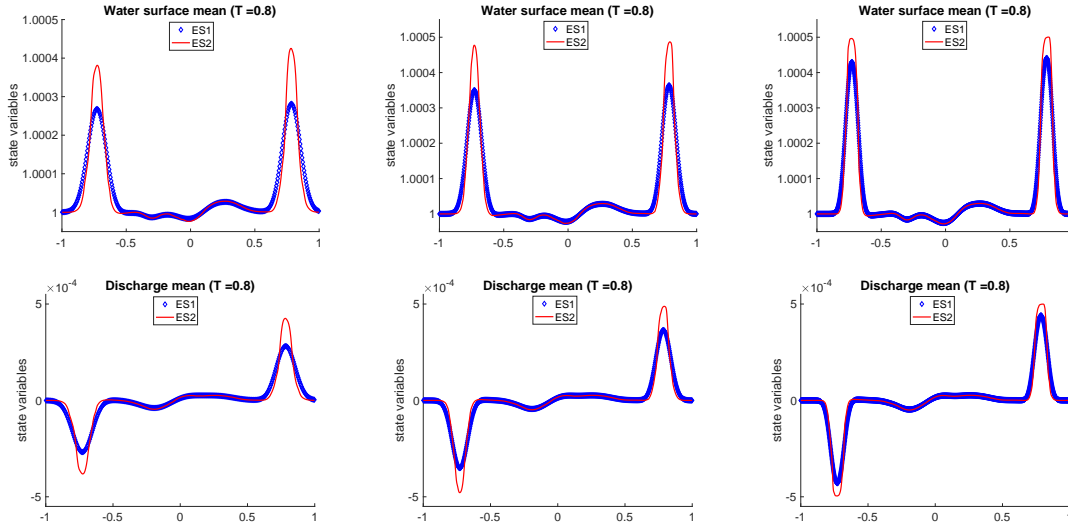


FIGURE 8. Results for section 5.3. Top: water surface mean, Bottom: discharge mean: Left: ES1 vs. ES2 on mesh $n_x = 400$. Middle: ES1 vs. ES2 on mesh $n_x = 800$. Right: ES1 vs. ES2 on mesh $n_x = 1600$. PC basis functions $K=9$.

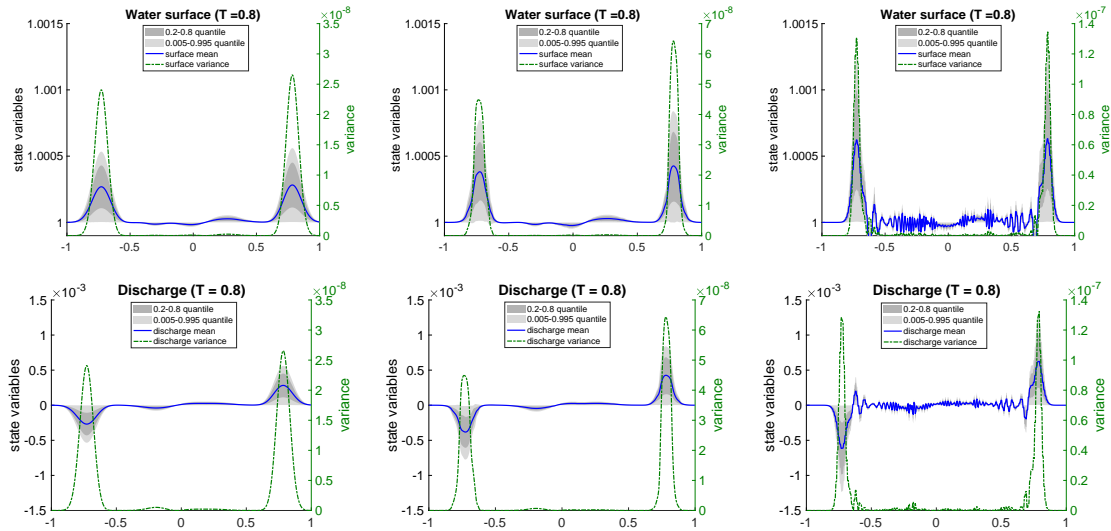


FIGURE 9. Comparison of the results for section 5.3 using different schemes. Top: water surface. Bottom: discharge. Left: ES1, Middle: ES2, Right: EC. Mesh $n_x = 400$ with $K = 9$ at time $T = 0.8$.

15. Ulrik S Fjordholm, Siddhartha Mishra, and Eitan Tadmor, *Well-balanced and energy stable schemes for the shallow water equations with discontinuous topography*, Journal of Computational Physics **230** (2011), no. 14, 5587–5609.
16. ———, *Arbitrarily high-order accurate entropy stable essentially nonoscillatory schemes for systems of conservation laws*, SIAM Journal on Numerical Analysis **50** (2012), no. 2, 544–573.
17. Sigal Gottlieb, Chi-Wang Shu, and Eitan Tadmor, *Strong Stability-Preserving High-Order Time Discretization Methods*, SIAM Review **43** (2001), no. 1, 89–112.
18. Alexander Kurganov, *Finite-volume schemes for shallow-water equations*, Acta Numerica **27** (2018), 289–351.

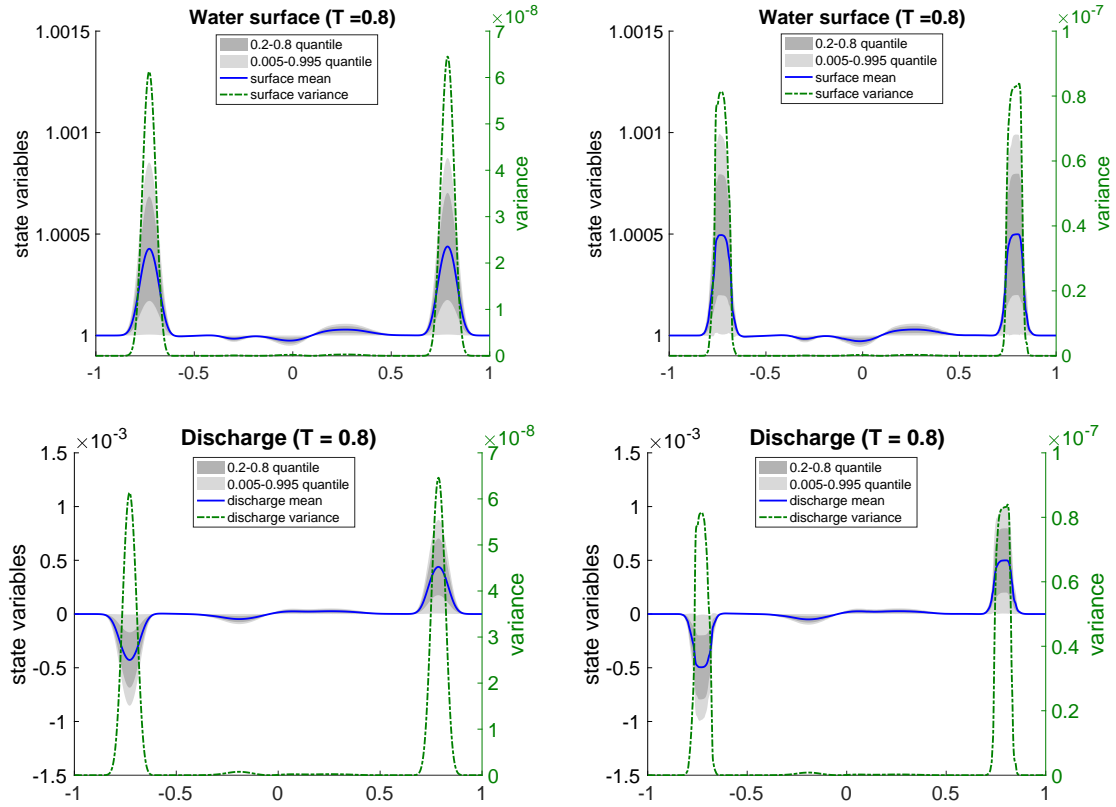


FIGURE 10. Comparison of the results for section 5.3 using different schemes. Top: water surface. Bottom: discharge. Left: ES1, Right: ES2. Mesh $n_x = 1600$ with $K = 9$ at time $T = 0.8$.

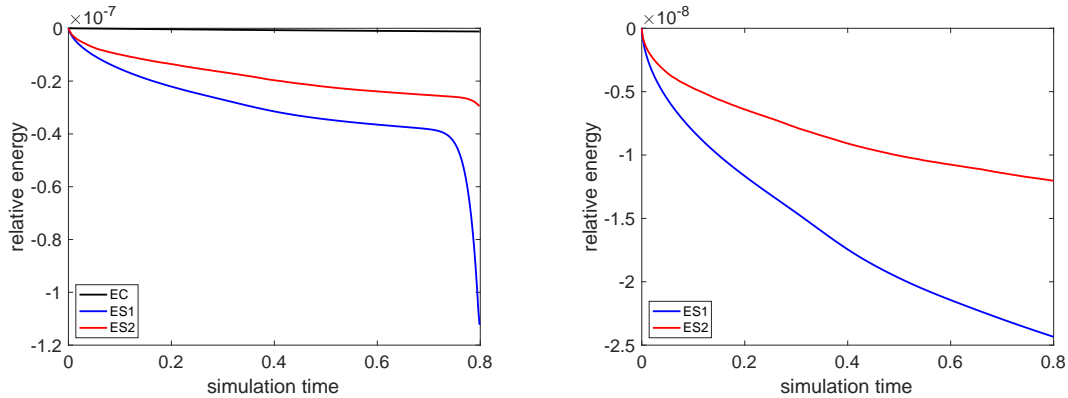


FIGURE 11. Comparison of the results for section 5.3 using different schemes. Relative energy change: Left: EC vs. ES1 vs. ES2 on mesh $n_x = 400$. Right: ES1 vs. ES2 on mesh $n_x = 1600$.

19. Alexander Kurganov and Doron Levy, *Central-Upwind Schemes for the Saint-Venant System*, ESAIM: Mathematical Modelling and Numerical Analysis **36** (2002), no. 3, 397–425.
20. Alexander Kurganov and Guergana Petrova, *A Second-Order Well-Balanced Positivity Preserving Central-Upwind Scheme for the Saint-Venant System*, Communications in Mathematical Sciences **5** (2007), no. 1, 133–160.
21. Randall J. LeVeque, *Numerical Methods for Conservation Laws*, Springer, 1992 (en).
22. ———, *Finite Volume Methods for Hyperbolic Problems*, Cambridge University Press, 2002.
23. Xin Liu, Jason Albright, Yekaterina Epshteyn, and Alexander Kurganov, *Well-balanced positivity preserving central-upwind scheme with a novel wet/dry reconstruction on triangular grids for the Saint-Venant system*, Journal of Computational Physics **374** (2018), 213–236.
24. Benedict D. Rogers, Alistair G. L. Borthwick, and Paul H. Taylor, *Mathematical balancing of flux gradient and source terms prior to using Roe’s approximate Riemann solver*, Journal of Computational Physics **192** (2003), no. 2, 422–451.
25. Ralph C. Smith, *Uncertainty Quantification: Theory, Implementation, and Applications*, SIAM-Society for Industrial and Applied Mathematics, Philadelphia, 2013.
26. Timothy John Sullivan, *Introduction to Uncertainty Quantification*, vol. 63, Springer, 2015.
27. Eitan Tadmor, *The numerical viscosity of entropy stable schemes for systems of conservation laws. i*, Mathematics of Computation **49** (1987), no. 179, 91–103.
28. ———, *Entropy stability theory for difference approximations of nonlinear conservation laws and related time-dependent problems*, Acta Numerica **12** (2003), 451–512.
29. Y. Xing, *Chapter 13 - Numerical Methods for the Nonlinear Shallow Water Equations*, Handbook of Numerical Analysis (Rémi Abgrall and Chi-Wang Shu, eds.), Handbook of Numerical Methods for Hyperbolic Problems, vol. 18, 2017, pp. 361–384.
30. Yulong Xing, *High order finite volume WENO schemes for the shallow water flows through channels with irregular geometry*, Journal of Computational and Applied Mathematics **299** (2016), 229–244.
31. Yulong Xing and Chi-Wang Shu, *High order finite difference WENO schemes with the exact conservation property for the shallow water equations*, Journal of Computational Physics **208** (2005), no. 1, 206–227.
32. ———, *High order well-balanced finite volume WENO schemes and discontinuous Galerkin methods for a class of hyperbolic systems with source terms*, Journal of Computational Physics **214** (2006), no. 2, 567–598.
33. ———, *A new approach of high order well-balanced finite volume WENO schemes and discontinuous galerkin methods for a class of hyperbolic systems with source terms*, Communications in Computational Physics **1** (2006), no. 1, 100–134.
34. Dongbin Xiu, *Numerical methods for stochastic computations: A spectral method approach*, Princeton university press, 2010.
35. J. G. Zhou, D. M. Causon, C. G. Mingham, and D. M. Ingram, *The Surface Gradient Method for the Treatment of Source Terms in the Shallow-Water Equations*, Journal of Computational Physics **168** (2001), no. 1, 1–25.
36. Nelida Črnjarić Žic, Senka Vuković, and Luka Sopta, *Balanced finite volume WENO and central WENO schemes for the shallow water and the open-channel flow equations*, Journal of Computational Physics **200** (2004), no. 2, 512–548.

(Dihan Dai) SAN DIEGO, CA, USA
 Email address: dihandai2022@gmail.com

(Yekaterina Epshteyn) DEPARTMENT OF MATHEMATICS, THE UNIVERSITY OF UTAH, SALT LAKE CITY, UT 84112, USA
 Email address: epshteyn@math.utah.edu

(Akil Narayan) DEPARTMENT OF MATHEMATICS AND SCIENTIFIC COMPUTING AND IMAGING (SCI) INSTITUTE, THE UNIVERSITY OF UTAH, SALT LAKE CITY, UT 84112, USA
 Email address: akil@sci.utah.edu